



Petrogenesis and metallogenesis of an extraordinary deeply hidden granite pluton overlain by W-Zn-Pb-Ag-mineralized roof: Example from Xidamingshan district, South China



Yangyang Feng ^{a,b}, Wei Fu ^{a,*}, Zuohai Feng ^{a,*}, Jianwen Yang ^b, Zhongyang Li ^c, Xingwen Le ^c, Saisai Li ^a, Meng Feng ^a, Chunzeng Wang ^d, Jifeng Xu ^e

^a Guangxi Key Laboratory of Hidden Metallic Ore Deposits Exploration, College of Earth Sciences, Guilin University of Technology, Guilin 541004, China

^b School of the Environment, University of Windsor, Windsor N9B 3P4, Canada

^c Guangxi Zhuang Autonomous Region Geological and Mineral Exploration Bureau, Nanning 530023, China

^d University of Maine at Presque Isle, Presque Isle, Maine, USA

^e College of Earth Sciences and Resources, China University of Geosciences, Beijing 100083, China

ARTICLE INFO

Keywords:

Hidden granite pluton
Geochronology
Petrogenesis
W-Pb-Zn-Ag deposits
Xidamingshan
South China

ABSTRACT

Common understanding of pluton-related W-polymetallic mineralization is mainly based on studies in areas with exposed granitic plutons or plutons buried at shallow levels. However, there exist a large number of ore deposits that are considered to be associated with deeply hidden granitic plutons (deeper than 500 m). Their metallogenesis is not well documented due to lack of deep drilling and sampling. In this paper, we present a deeply hidden granitic pluton recently discovered by a kilometer-scale drilling project in the Xidamingshan Mountains area in western South China. The pluton, here referred to Xidamingshan granitic pluton, underlies the Xidamingshan W-Zn-Pb-Ag-mineralized district. Petrographic examinations reveal that the hidden granite is biotite granite with partly hydrothermal alteration and that the upper part of the pluton is subjected to greisenization. Geochronological analyses indicate that the granite pluton was emplaced at the Late Cretaceous time with zircon U-Pb ages of 98.0 ± 1.0 Ma and 99.8 ± 0.9 Ma. The emplacement was subsequently followed by hydrothermal activity as indicated by muscovite ^{40}Ar - ^{39}Ar ages of 93 ± 3 Ma and 92 ± 3 Ma. Re-Os dating of molybdenite yields an isochronal age of 95.9 ± 1.7 Ma (MSWD = 2.2). These ages indicate that the Xidamingshan mineralization is temporally related to the hidden granite. The granite is strongly peraluminous ($\text{A/CNK} = 1.50 - 1.61$) with high-K calc-alkaline affinity ($\text{ASI} = 1.46 - 1.61$) and shows enrichment in Rb, Ta, U, and K and depletion in Nb, P, and Ti. It contains muscovite and biotite but is lack of hornblende. It shows a steady correlation between P_2O_5 and increasing SiO_2 , high Rb/Sr ratios ($1.33 - 3.12$), and high zirconium saturation temperature (average of 767°C). The Xidamingshan granite is thus a typical S-type granite. Geochemical signature and negative $\epsilon_{\text{Hf}}(\text{t})$ values (-4.9 – -12.6) indicate that the hidden granite might have been generated by melting of crustal materials of argillaceous-depleted sedimentary rocks. Granites with such geochemical characteristics are known as having W-polymetallic mineralization specialization based on comparison with other ore-forming granites in South China. Significant W-polymetallic mineralization has been found within the thick Cambrian strata overlying the hidden granite pluton. Distribution of the related deposits demonstrates a typical zoning pattern from skarn-type W deposits, through vein-type Pb-Zn deposits, to vein-type Ag deposits. Given the combined evidences of metallocenic specialization of the source rocks for granitic magmas, geochronological coupling of the magmatism and hydrothermal activity, and the hydrothermal alteration and mineralization zoning, it is suggested that there exists a hydrothermal W-Zn-Pb-Ag mineralization system driven by the emplacement of the Late Cretaceous S-type hidden granite pluton. The findings of this study provide insights into future deep drilling and related ore exploration in regions with hidden granite in South China and the world.

* Corresponding authors.

E-mail addresses: fawei@glut.edu.cn (W. Fu), fzh@glut.edu.cn (Z. Feng).

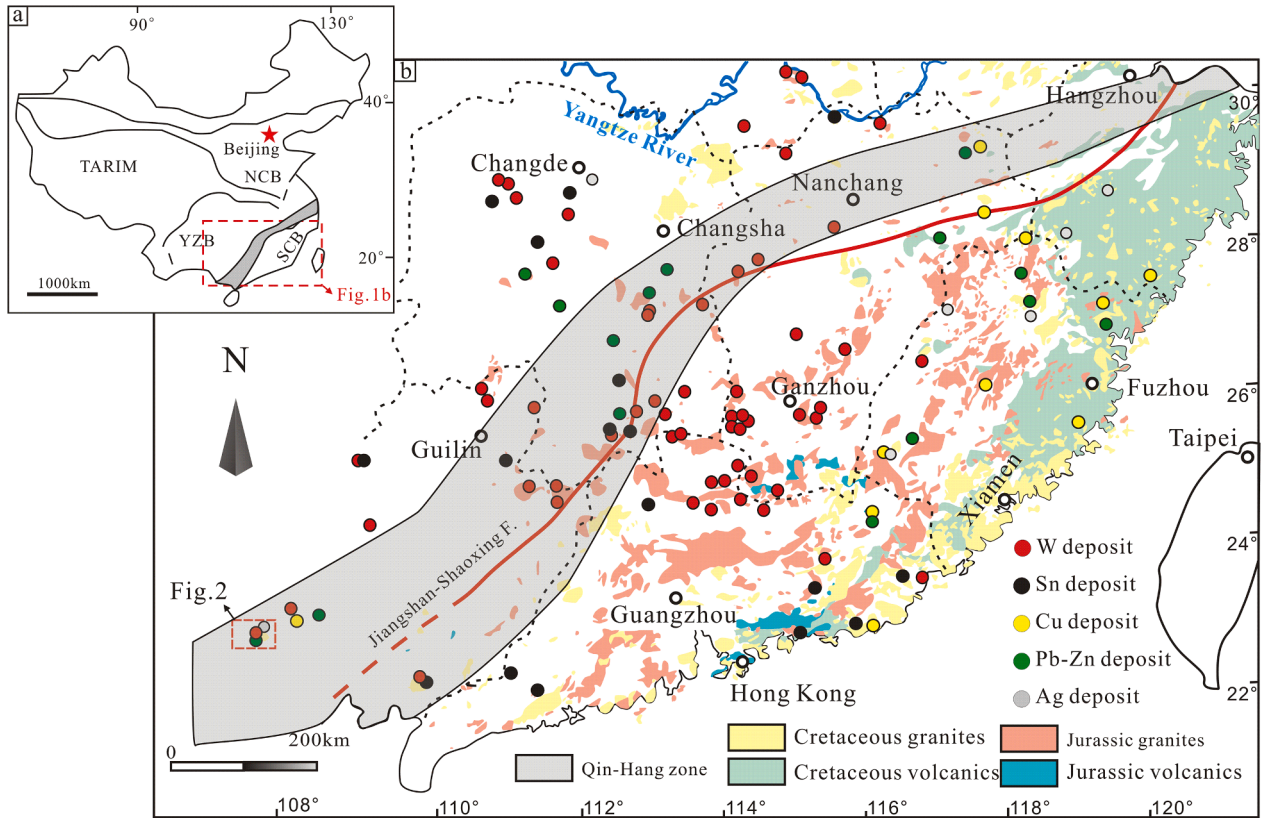


Fig. 1. (a) Sketch map of plate tectonics in China. TRAIM: Tarim block; NCB: North China Block; YZB: Yangtze Block. (b) Geology and distribution of the Mesozoic granitic plutons and related W-Sn-Cu-Pb-Zn-Ag ore deposits in South China (modified after Cai et al., 2017; Mao et al., 2011).

1. Introduction

South China is one of the most profitable regions for polymetallic ore production in the world and has been of interest to geologists for a long time (Fig. 1a) (e.g., Wang and Zhou, 2005; Jiang et al., 2006; Sun, 2006; Pirajno, 2013; Huang et al., 2017a). Geologically, this region is characterized by intensive tectonic activities and periodic granitic magmatic events during Paleozoic and Mesozoic eras (Charvet et al., 1990; Maruyama et al., 1997) that created geologic conditions favorable for formation of abundant endogenous non-ferrous and precious metal deposits (Xu et al., 1984; White, 2002; Goldfarb et al., 2004; Wang et al., 2004, 2014; Duan et al., 2011; Lees et al., 2011; Mao et al., 2011; Zhong et al., 2013a; 2013b; Lecumberri-Sánchez et al., 2014; Chen et al., 2015). Extensive magmatism, in particular in the Mesozoic, generated voluminous granitoids that are spatially and genetically associated with W, Sn, Cu, Mo, Pb, Zn, Ag, Au and Sb mineralization (Fig. 1b).

In terms of occurrence, most of the ore-forming granitoids crop out due to significant weathering and erosion, for example, the granitic plutons at Nanyangtian W deposit (Zhang et al., 2012), Xianghualing Sn-Nb-Ta deposit (Yuan et al., 2008b; 2008c), Yaogangxian W-Mo deposit (Hu et al., 2012a), Shizhuyuan W-Sn-Mo-Bi deposit (Mao and Li, 1995; Mao et al., 1995a; 1996a; 1996b), Furong Sn deposit (Mao et al., 2004; Peng et al., 2006; 2007; 2011; Yuan et al., 2008a) and Xihuashan W deposit (Guo et al., 2012; Hu et al., 2012c; Yang et al., 2013). However, there are a number of known ore-forming granitoids that occur as unexposed, hidden plutons. Examples include the plutons at Dachang Sn-polymetallic deposit (Wang et al., 2004; Cai et al., 2006), Gejiu Sn-polymetallic deposit (Cheng et al., 2010; 2013; Zhao and Li, 1987), Yuanzhudeng Cu-Mo deposit (Hu et al., 2013; Zhong et al., 2013a; 2013b), Baoshan Cu deposit (Bi et al., 2015) and Zhaibao Cu deposit (Yu et al., 2014). The ore-forming hidden granite plutons are considered to have better preservation condition for ore deposits than their exposed

counterparts, since the deposits are not affected by any significant surficial weathering and erosion. Thus, various mineralization types and complete mineralization systems are expected to occur within or around the hidden granite plutons (Jin et al., 2010). As Yuan et al. (1990) suggested, hidden granite-related ore deposits could be divided into two major mineralization patterns. The ore bodies of the first pattern are mainly hosted in the strata overlying the hidden granite plutons, whereas those of the second pattern are hosted within the hidden granite plutons.

The Xidamingshan region, located in western South China (Fig. 1b), is a critical mineral prospecting district in China. The Xidamingshan district where a number of W, Pb, Zn, Ag deposits have been discovered over the years (Fig. 2a, b; e.g., Cui et al., 2000; Xiao et al., 2018a–c; Zhang et al., 2015; Lei, 2012; Li et al., 2016), however, is lack of exposed granitic plutons except for a few of felsic dikes at the summit of the Xidamingshan Mountain and several diabase dikes in the surrounding areas. Previous geological, geophysical and geochemical investigations suggest that there may exist a large hidden granitic pluton underlying the deposits of the Xidamingshan region (Zhu et al., 1989; Mai et al., 1990; Liang and Yang, 2004; Huang, 1994; 2008). Until recently, a kilometer-scale deep borehole drilling project confirmed the presence of such a hidden granite pluton, specifically in the Luowei area. However, the question of whether the hidden granite contributed to the regional mineralization, as previous researchers speculated (Huang, 1994; Lei, 2012; Li et al., 2016), remains unresolved.

In this paper, we present new data of geochronology, whole-rock geochemistry of major and trace elements and zircon Hf isotopes from the hidden granite pluton, with an objective of unveiling its petrogenesis and metallogenic significance. Given the fact that there are abundant hidden granite plutons in adjacent regions (Zhu et al., 1989; Mai et al., 1990; Huang, 2008), and to a larger extent in South China, our results would help shed light on predicting hidden granite plutons and mineral

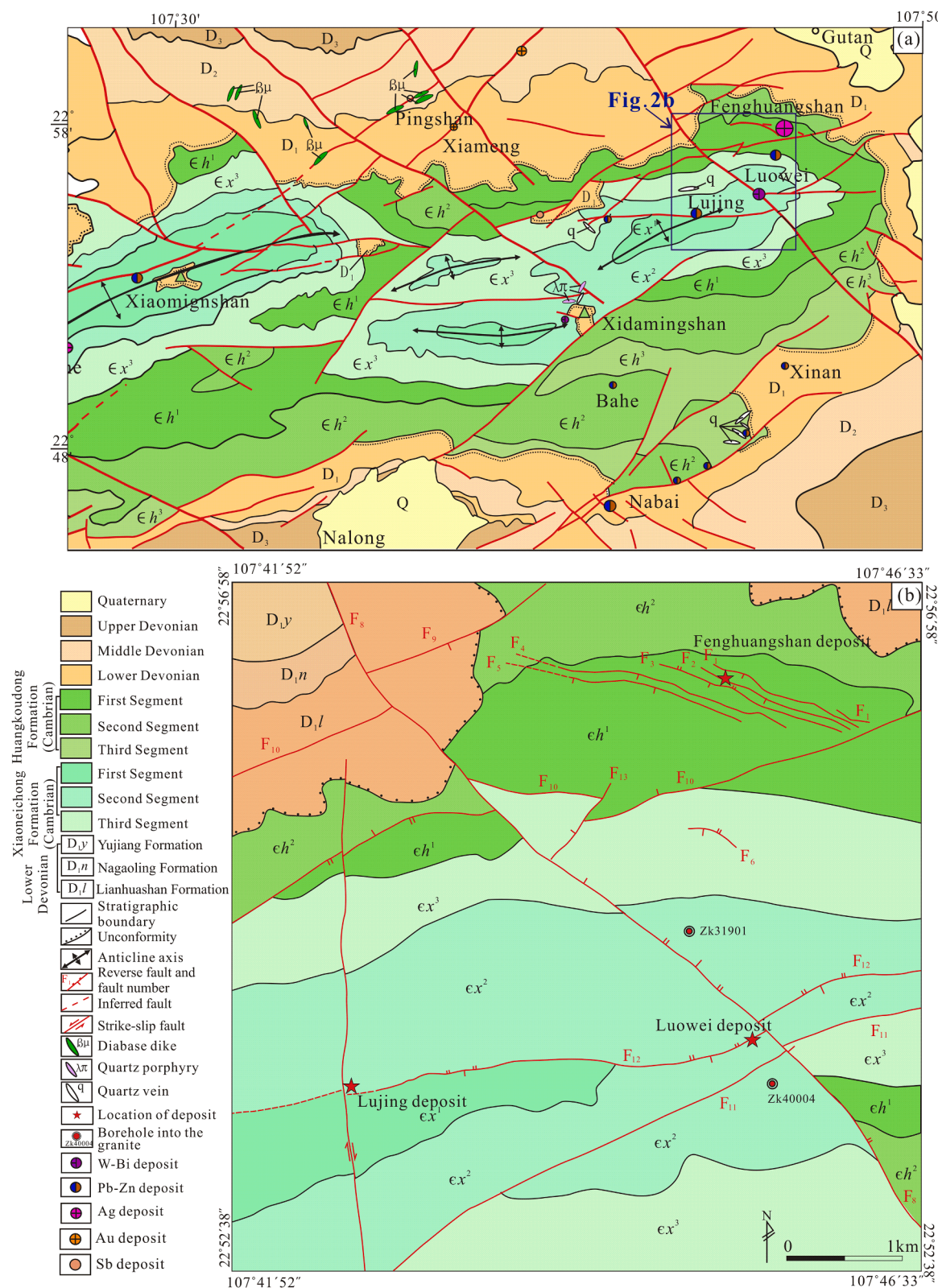


Fig. 2. Regional geologic map of the Xidamingshan anticlinorium (a) and schematic geologic map of the Xidamingshan orefield (b) (modified after Li et al., 2016).

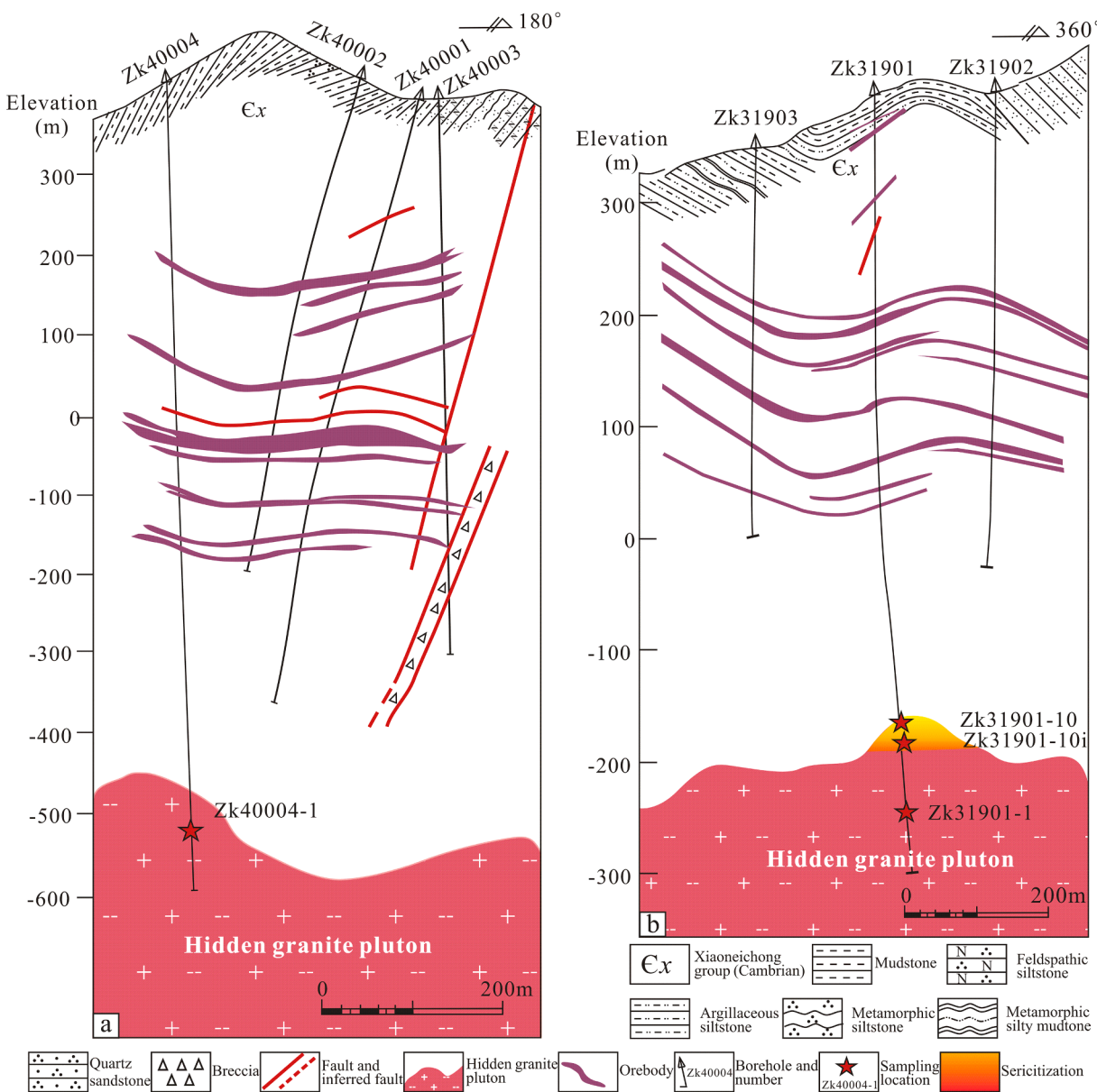


Fig. 3. Cross-section showing the hidden granite and related W-polymetallic deposits hosted in its overlying strata (modified after Huang et al., 2015).

exploration in similar geological context.

2. Geological setting

The study area is located in the southwest of the Qinhang tectono-metallogenic belt, in Guangxi, South China. The tectono-metallogenic belt occurs along the Neoproterozoic suture zone between the Yangtze Block in the northwest and the Cathaysia Block in the southeast (Fig. 1; Chen and Jahn, 1998; Li et al., 2002; Zhou et al., 2012). It extends from the Jiangshan-Shaoxing fault zone in Zhejiang and Jiangxi provinces in the northeast, through the Chaling-Chenzhou-Linwu fault zone in Hunan Province, to the area of Beibowan Bay in Guangxi Zhuang Autonomous Region in the southwest (Shu et al., 2011; Zhou et al., 2015; Zhao et al., 2017a; 2017b). After the Neoproterozoic amalgamation, the South China Block has experienced episodic tectono-magmatic events during the Caledonian (middle Paleozoic), Indosinian (Triassic) and Yanshanian (Jurassic-Cretaceous) orogenies (Yuan et al., 2015). In the late Mesozoic time, the northwest-directed subduction of the Paleo-Pacific (or Izanagi) plate beneath the Eurasian continent (Zhou and Li, 2000;

Mao et al., 2011; 2013; Hu et al., 2017) generated complicated structural patterns and widespread granitoids. A large number of W-(Mo)-Pb-Zn-Au-Ag polymetallic deposits occur along the Qinhang tectono-metallogenic belt and adjacent areas (Fig. 1 b).

The entire Xidamingshan district is underlain by an E-W-trending anticlinorium (Fig. 2a). The anticlinorium is made of Cambrian flysch strata, including Xiaoneichong and Huangdongkou formations. The Xiaoneichong Formation mainly consists of mudstone, siltstone, and interbedded with lenses of limestone. The Huangdongkou Formation consists of sandstone interbedded with siltstone. Both the Xiaoneichong and Huangdongkou formations were deformed and metamorphosed during the Silurian Caledonian Orogeny at lower greenschist facies, forming abundant folds and E-W-striking thrust faults (Guangxi BGMR, 1985). The subsequent Late Triassic to Permian Indosinian Orogeny resulted in NEE-striking faults (Chen et al., 2011; Li et al., 2016). The anticlinorium is flanked by Devonian strata of Lianhuashan, Nagaoling and Yujiang formations of conglomerate, sandstone, marl, limestone, dolomite and dolomitic limestone (Fig. 2b). A large number of economic mineral deposits have been discovered in the Cambrian strata, as Liang

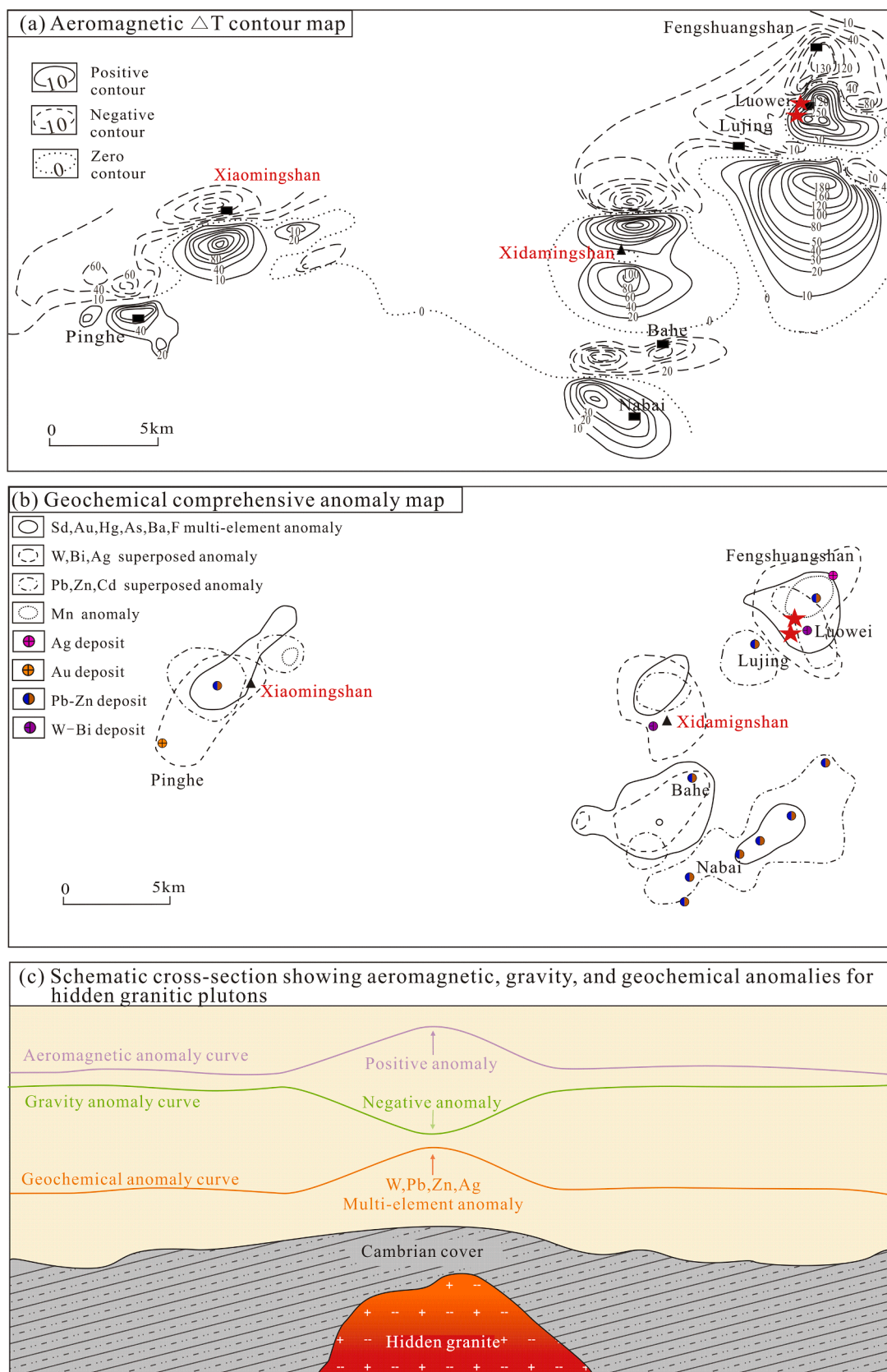


Fig. 4. (a) Simplified aeromagnetic map showing position of the Xidamingshan hidden granite pluton based on positive aeromagnetic anomaly; (b) A conceptual cross section showing aeromagnetic, gravity, and geochemical anomalies used for predicting hidden granite plutons; (c) Simplified geochemical map showing position of the Xidamingshan hidden granite pluton based on elemental comprehensive anomaly (Figures a, c are modified after Li et al., 2016).

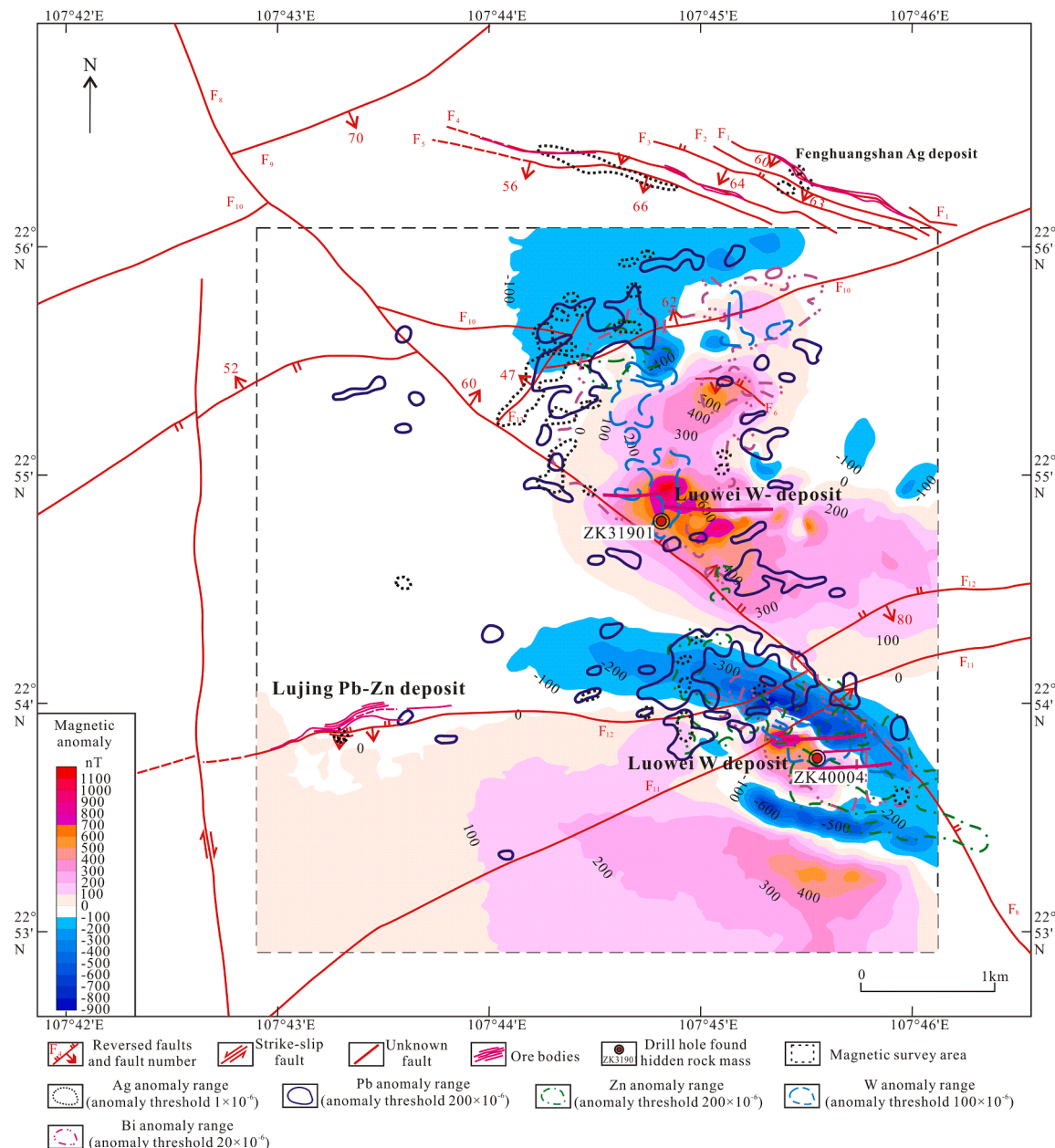


Fig. 5. Geophysical and geochemical anomaly map of the Luowei Orefield (modified after Guangxi No. 4 Geological Team).

and Yang (2004) reported that the Cambrian strata show high contents of ore-forming elements such as Pb, Zn and Ag (with concentration factors ranging from 1.5 to 3) (Fig. 2b). Among them, the Luowei deposit is a medium-scale W deposit accompanied by Zn and Bi mineralization. More than twelve W-Zn ore bodies have been found at this deposit (Fig. 3). Most of the ore bodies occur in stratiform and are spatially associated with skarns. In addition, a small part of the ore occurs as quartz stockwork (Zhang et al., 2015). In addition to skarn-type and hydrothermal vein-type W-Zn deposits, there are a number of mineral deposits that contain various metals. In the Xidamingshan district, there exists hydrothermal vein-types Pb-Zn deposits and Ag deposits (Lei, 2012; Li et al., 2016). The Pb-Zn mineralization is located along the E-W- and NEE-striking faults, such as the Nongtun, Changtun, Lujing, and Nabai deposits. The deposits are hosted by both Xiaoneichong and Huangdongkou formations, and are fracture-controlled. The ore bodies are mainly found in fractures filled with quartz and carbonate veins and have a large dip angle (Chai et al., 2015; Li et al., 2017). The Ag mineralization is found in Fenghuangshan and Pinhe districts. Notably,

the Fenghuangshan Ag deposit is the largest independent Ag deposit ever found in China. The ore bodies are strictly bound to deep fractures and associated with silica and carbonate alterations. The main Ag-bearing minerals include pyrargyrite, canfieldite, miargyrite, ramdohrite, freieslebenite, stephanite and freibergite that coexist with galena, alabandite, and sphalerite (Lu, 2015).

3. Occurrence of the hidden granite pluton

Generally, to predict the mode of occurrence of hidden granite plutons, geophysical surveys including gravity, magnetic and electric methods are proven to be effective (Jin et al., 2010). For the Xidamingshan region, geophysical surveys have been conducted in order to determine the location of the hidden granite pluton underlain the thick Cambrian strata (Zhu, 1989; Mai et al., 1990; Huang, 2008). Gravity survey (Mai et al., 1990) reveals two significant negative anomalies within the study area, the west and east anomalous zones, respectively. The east anomalous zone strides across the summit of the Xidamingshan

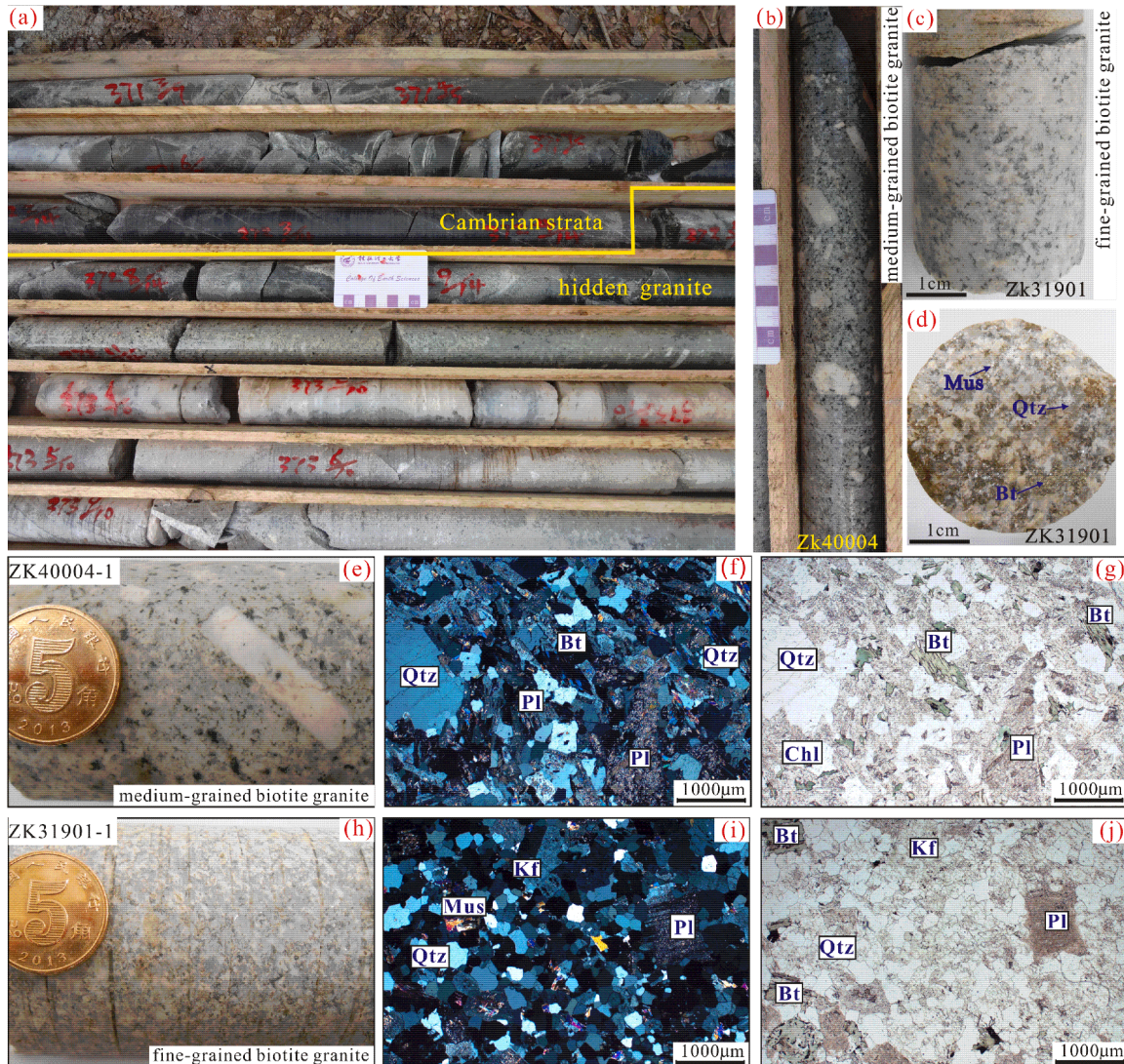


Fig. 6. Field photographs and photomicrographs of the granite. (a) Contact between country rocks and the hidden granite; (b) Core sample of muscovite-bearing skarn ore for muscovite Ar-Ar analysis; (c) Samples of molybdenite-bearing quartz vein for Re-Os analysis; (d) Core sample of medium-grained biotite granite (Zk40004-1); (e) Photomicrograph of biotite granite Zk40004; (f) Photomicrograph of biotite granite Zk40004; (g) Core sample of fine-grained biotite granite (Zk31901-1); (h) Photomicrograph of biotite granite Zk31901; (i) Photomicrograph of biotite granite Zk31901; Bt - biotite; Chl - chlorite; Kfs - potassium feldspar; Mol - Molybdenite; Ms - Muscovite; Pl - plagioclase; Py - Pyrite; Qz - Quartz. (f) and (i) are under cross-polarized light; (g) and (j) are under plane-polarized light.

Mountain with a length of nearly 55 km, and the west anomalous zone occurs on the western side of the Xiaomingshan Mountain with a 75 km length. The presence of negative gravity anomaly is thought to be generated by the occurrence of a hidden granite pluton (with an average density value = 2.72 g/cm³) due to its lower density compared to that of surrounding sedimentary strata (with an average density value = 2.61 g/cm³) (Guangxi GSI, 1984). Zhu (1989) further conducted aeromagnetic survey and delineated two positive aeromagnetic anomalous zones (Fig. 4a, c), which are spatially correspondent to both the east and west gravity anomalous zones. Generally, the presence of positive aeromagnetic anomalies can be caused by hidden granitic plutons based on content of preferred magnetic minerals within the granite (Huang, 2008). In addition, according to 1:200000-scale soil geochemical mapping results (Fig. 4b, c), several anomalies of major non-ferrous and precious metal elements (e.g., W, Bi, Pb, Zn, Au, Ag, Sb, and Hg) are discovered in the areas of Fenghuangshan-Luowei, Xidamingshan, Lumei, Xin'an-Nabai and Xiaomingshan. They are spatially coincident with the gravity and aeromagnetic anomalies (Fig. 4a, b, c). Especially in the Luowei district, surface geochemical exploration has revealed a typical W-Bi-Zn-Pb-Ag anomaly area, which extends radially from the

inner zone with W-Bi anomaly through the middle zone with Zn-Pb anomaly to the outer zone with Ag anomaly. This geochemical anomaly area is well correspondent to the aeromagnetic anomalies (Fig. 5).

Yang et al. (2017) conducted a detailed simulation and inference on the three-dimensional shape of the hidden granite pluton by gravity and magnetic inversions. The results show that the hidden granite pluton trends nearly in East-West direction, with a length of about 40 km and a width of about 30 km. As Zhu (1989); Mai et al. (1990); Huang (2008) suggested, the Xidamingshan hidden pluton is made of the Xidamingshan body in the west and the Xiaominshan body in the east. Both bodies might be connected at about 13 km in depth, forming a big saddle-shaped batholith (Yang et al., 2017). Specifically, the Xidamingshan body is relatively shallower (but still greater than 500 m in depth), with its top estimated at a depth of 600 m, 800 m and 1000 m in Fenghuangshan, Damingshan and Lumei areas, respectively. In contrast, the Xiaomingshan body is relatively deeper (greater than 900 m in depth) with its top estimated at a depth of 900 m and 1,000 m at Pinghe and Xiaomingshan areas, respectively.

Table 1

Analytical data of major elements (wt%) for Xidamingshan hidden pluton.

Sample	ZK40004-1	ZK40004-5	ZK40004-6	ZK40004-7	ZK40004-4	ZK31901-3	ZK31901-1	ZK31901-7	ZK31901-4
SiO ₂	72.41	71.04	71.28	72.43	71.36	70.09	71.07	71.81	71.44
Al ₂ O ₃	14.29	14.10	14.38	14.13	14.22	14.79	14.25	13.32	14.11
FeO	1.21	1.26	1.36	1.02	1.17	1.52	1.36	1.30	1.05
Fe ₂ O ₃	1.53	1.85	1.86	1.74	1.62	2.04	2.14	1.81	1.83
MgO	0.63	0.79	0.69	0.63	0.65	0.79	0.70	0.68	0.74
CaO	1.45	1.72	1.38	1.25	1.38	2.25	2.05	0.92	2.01
Na ₂ O	4.23	4.27	3.89	3.38	4.23	4.49	4.06	2.76	4.09
K ₂ O	3.60	3.39	3.64	4.49	3.78	2.61	2.81	5.47	2.88
MnO	0.05	0.07	0.05	0.05	0.05	0.07	0.07	0.06	0.08
TiO ₂	0.27	0.32	0.27	0.25	0.30	0.31	0.30	0.32	0.31
P ₂ O ₅	0.16	0.19	0.16	0.18	0.16	0.20	0.15	0.18	0.15
LOI	1.37	2.23	2.29	1.45	2.25	2.34	2.38	2.66	1.99
Total	99.98	99.97	99.89	99.97	99.99	99.98	99.98	99.98	99.64
Qz	30.18	28.79	31.07	32.30	28.84	28.25	31.50	32.47	31.65
An	6.17	7.39	5.87	5.07	5.87	9.92	9.27	3.43	9.10
Ab	35.86	36.50	33.27	28.74	36.19	38.32	34.73	23.68	35.08
Or	21.31	20.24	21.74	26.66	22.59	15.56	16.79	32.78	17.25
C	1.18	0.73	1.93	1.87	1.06	0.98	1.18	1.64	0.99
R1	2404	2357	2449	2508	2312	2382	2563	2469	2583
R2	467	505	469	444	464	575	539	399	536
AR	2.98	2.88	2.83	2.57	3.11	2.43	2.46	2.27	2.52
AKI	0.55	0.54	0.52	0.56	0.56	0.48	0.48	0.62	0.49
DI	87.35	85.53	86.08	87.70	87.62	82.13	83.02	88.93	83.98
K/N	0.85	0.79	0.94	1.33	0.89	0.58	0.69	1.98	0.70
A/NK	1.83	1.84	1.91	1.80	1.78	2.08	2.07	1.62	2.02
A/CNK	1.54	1.50	1.61	1.55	1.51	1.58	1.60	1.46	1.57

AKI=(Na₂O + K₂O)/Al₂O₃; K/N = Na₂O/K₂O; A/CNK = Al₂O₃/(Na₂O + K₂O + Al₂O₃); DI- Differentiation index**Table 2**Analytical data of trace elements ($\times 10^{-6}$) for Xidamingshan hidden pluton.

Sample	ZK40004-1	ZK40004-5	ZK40004-6	ZK40004-7	ZK40004-4	ZK31901-3	ZK31901-1	ZK31901-7	ZK31901-4
Rb	332	321	342	381	339	237	240	385	288
Ba	585	686	826	641	569	678	746	730	650
Th	19.5	19.2	17.8	17.6	21.1	15.3	15.7	28.4	19.7
U	11.2	11.7	7.03	14.5	21.8	2.21	2.64	27	3.25
Ta	4.05	2.6	3.48	3.59	3.95	1.29	1.15	3.25	1.69
Nb	21.4	19.5	18.4	19.3	21.5	13	13.5	22.7	13.5
Pb	29.3	23.2	31.5	37.9	27.3	15.8	28.3	99.8	22.3
Sr	174	150	162	122	130	170	180	130	124
Zr	141	148	150	128	129	143	150	96.7	155
Hf	4.46	4.62	4.79	4.12	3.99	4.3	4.5	3.27	4.94
La	32.5	36.1	31.4	28.1	30.6	31.3	30.5	32.9	33.5
Ce	59	63.9	55.6	51.1	55.6	54.6	53.2	64.4	60.5
Pr	6.74	7.25	6.27	5.91	6.37	6.15	5.93	7.63	6.84
Nd	25	26.3	22.9	22	23.7	22.7	21.7	29	25.6
Sm	4.56	4.68	4.12	4.1	4.35	3.85	3.73	5.46	4.41
Eu	0.68	0.71	0.67	0.59	0.6	0.74	0.68	0.47	0.75
Gd	3.29	3.61	3.14	3.18	3.2	3.14	2.82	4.19	3.32
Tb	0.55	0.55	0.53	0.57	0.52	0.49	0.44	0.67	0.47
Dy	2.65	2.54	2.25	2.55	2.56	2.31	2.04	3.04	2.22
Ho	0.42	0.41	0.41	0.44	0.46	0.35	0.36	0.47	0.37
Er	1.34	1.21	1.16	1.23	1.26	1.11	1.04	1.52	1.2
Tm	0.19	0.19	0.19	0.21	0.2	0.17	0.15	0.26	0.15
Yb	1.38	1.3	1.12	1.31	1.58	1.11	0.92	1.55	1.12
Lu	0.2	0.16	0.19	0.18	0.18	0.15	0.14	0.23	0.19
Y	13.5	12.2	12	12.6	13.1	11.5	10.1	14	10.5
Li	77.2	67.5	58.8	60.8	73	41.4	41.9	61.4	48
W	6.7	13.3	6.01	12	5.66	17.6	14.1	171	40.8
Bi	0.3	0.23	0.29	0.92	0.3	0.27	0.74	63	0.3
δ Eu	0.51	0.51	0.55	0.48	0.47	0.63	0.62	0.29	0.57
δ Ce	0.93	0.91	0.92	0.92	0.93	0.91	0.91	0.96	0.93
Σ REE	138.5	148.91	129.96	121.48	131.17	128.18	123.65	151.79	140.63
LREE	128.48	138.94	120.96	111.8	121.22	119.34	115.74	139.86	131.6
HREE	10.02	9.97	9	9.68	9.96	8.84	7.91	11.93	9.03
LREE/HREE	12.83	13.93	13.45	11.55	12.17	13.51	14.64	11.72	14.57
(La/Yb) _N	16.89	19.92	20.11	15.39	13.89	20.23	23.83	15.23	21.45

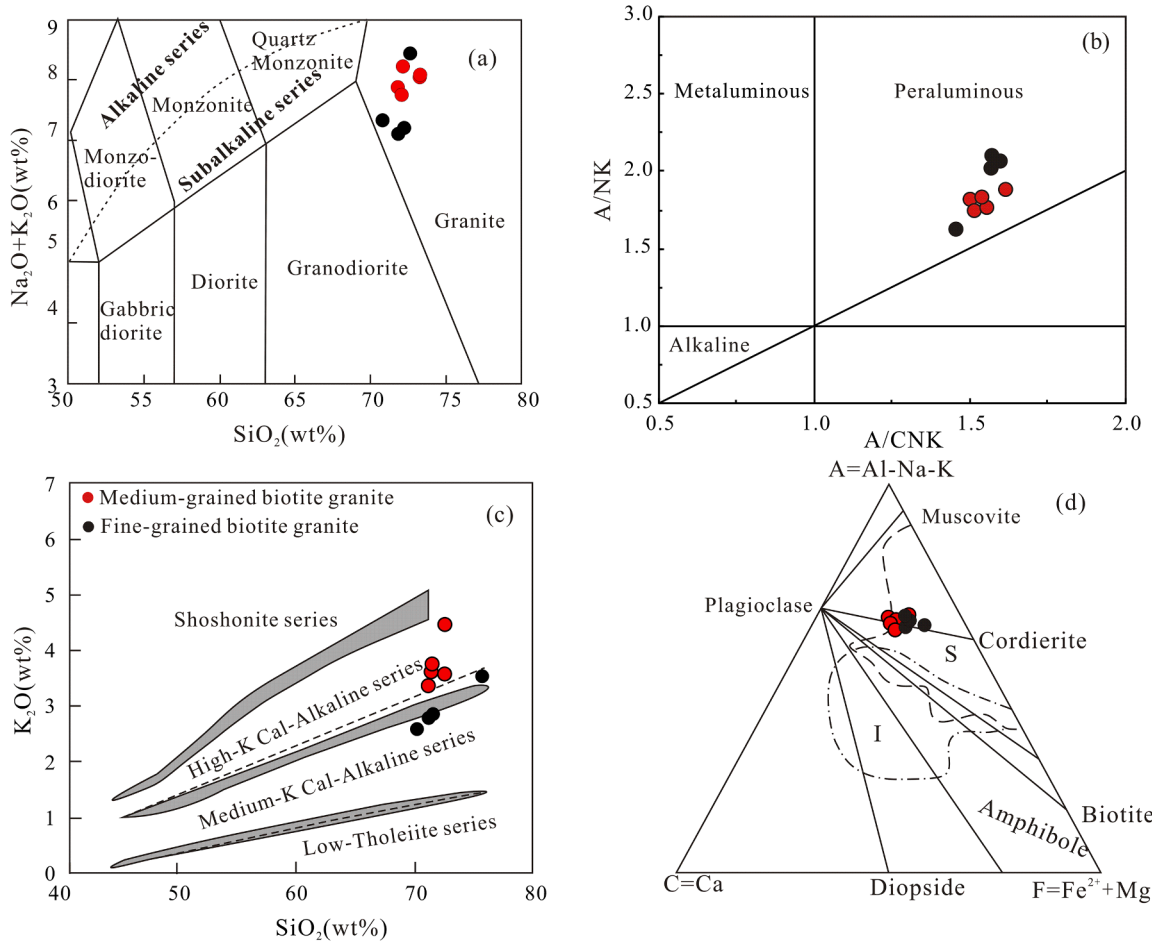


Fig. 7. (a) TAS classification diagram (after Middlemost, 1994); (b) ACNK vs. ANK diagram (after Maniar and Piccoli, 1989); (c) SiO₂ vs. K₂O diagram (after Peccerillo and Taylor, 1976); (d) ACF diagram (after Hine et al., 1978). See the text for interpretation.

4. Sampling and analytical methods

4.1. Sampling

A total of nine fresh granite samples were collected for major and trace elemental analyses, two granite samples for zircon geochronology and Hf isotopic analyses, two hydrothermal alteration muscovite samples for Ar-Ar dating, and eight molybdenite samples for Re-Os dating from drill holes ZK40004 and ZK31901. The granite samples from the deep drill hole (ZK40004, at 940 m) and shallow drill hole (ZK31901, at 650 m) have almost identical rock-forming mineral compositions, including quartz (25–30%), potassium-feldspar (20–25%), plagioclase (25–35%), biotite (5%), as well as trace amounts of muscovite, apatite, zircon and magnetite (Fig. 6d–i). It is a biotite granite. However, they are significantly different in textures. The samples from the deep drill hole show medium-grained texture with grains sized at 2–4 mm and with feldspar phenocrysts up to 10 mm in length. The samples from the shallower drill hole show a typical fine-grained texture with mineral size ranging at 0.5–1.5 mm. The samples used for dating show slight hydrothermal alteration such as greisenization, chloritization and skarnization. The skarnization alteration is closely related to tungsten mineralization in the Xidamingshan district.

Two muscovite samples (ZK31901-10 and ZK31901-10i) were separated from the 620 m and 622.5 m depth in borehole ZK31901 (Fig. 3b, b). Samples from the upper contact zone of the hidden granite pluton show euhedral to subhedral muscovite aggregates with their diameters of about 1–4 mm. They are relatively fresh and show no pleochroism. In the upper part of the pluton, as seen from ZK31901, the

samples have subjected to a greisenization alteration with various extents. Such a phenomenon is not observed in the samples from ZK40004. This indicates that the post-emplacement hydrothermal alteration might have occurred in the convex part of the hidden granite pluton.

Eight molybdenite samples from the wolframite-bearing quartz veins (drill holes of ZK40004 and ZK41602) in the Luowei deposit were selected for Re-Os dating. The ore-bearing quartz veins consist of quartz, wolframite, molybdenite and muscovite; and the molybdenite displays a flake-like texture along the margins of the veins (Fig. 6c).

4.2. Major and trace elements

Fresh samples were air dried, crushed, pulverized by agate mortar and sieved through a 200 mesh. The powder samples for major and trace elemental analyses were performed at the National Research Center for Geoanalysis in Beijing. Major elements were analyzed using X-ray fluorescence spectrometry (XRF), with analytical uncertainties below 5% (Zhang et al., 2009). The analytical precision for major oxides, based on certified standards (GSR-1, GSR-3) and duplicate analyses, is expressed in terms of relative percentages, ranging from $\pm 0.01\%$ to $\pm 0.20\%$. Trace elements were determined by solution ICP-MS. The detection limits of about several pg/g in solution, corresponding to a determination limit of about 10 ppb in solid samples for trace elements. The uncertainties of the ICP-MS analyses are estimated to be better than 5% (relative) for most trace elements with concentrations greater than 10 ppm and 10% for elements less than 10 ppm.

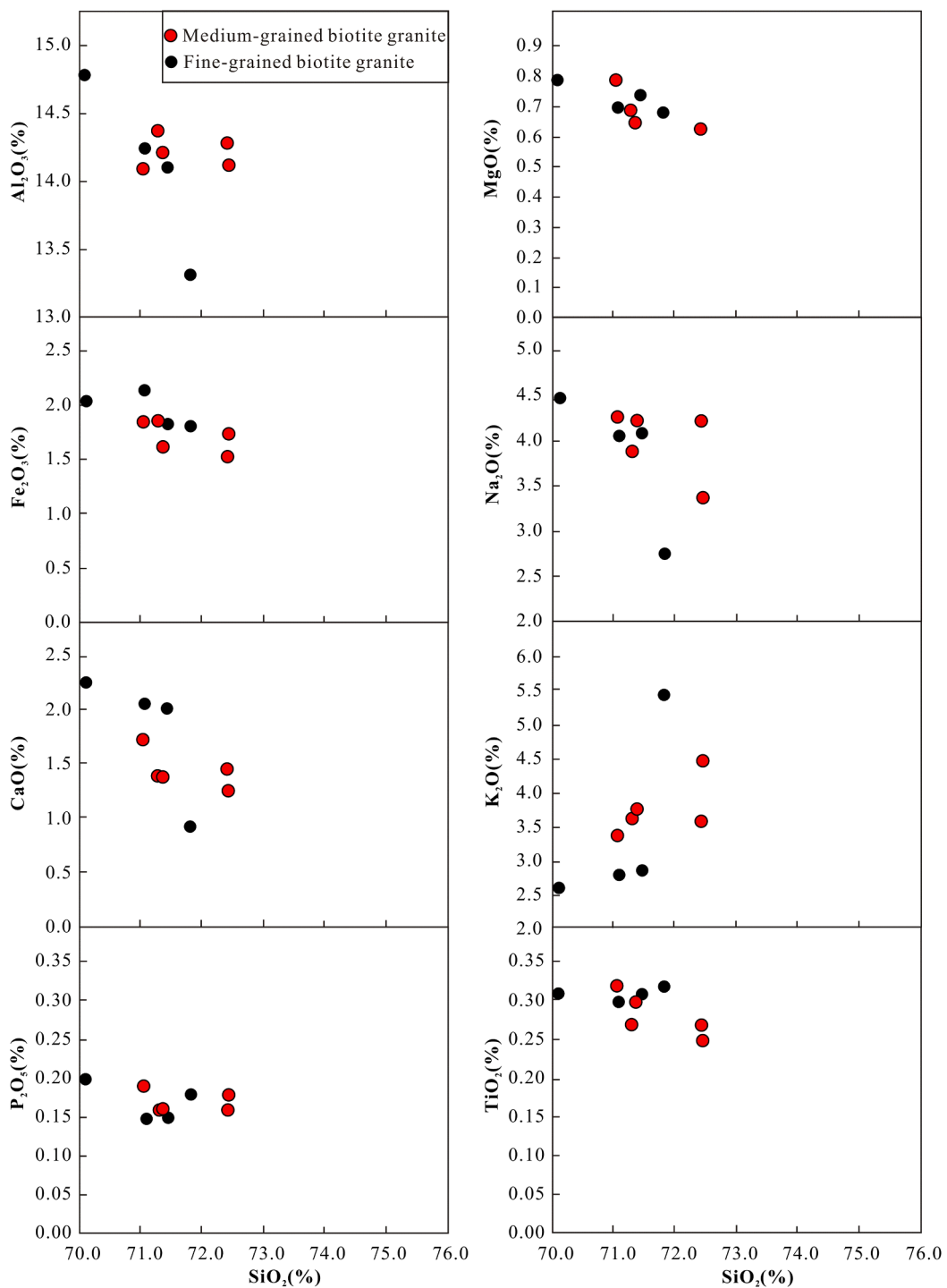


Fig. 8. Harker diagrams (SiO_2 vs. major oxides) for the Xidamingshan hidden granite.

4.3. Zircon U-Pb geochronology

The biotite granite samples (Zk40004-1 and Zk31901-1) for zircon U-Pb dating were collected from the drill holes of Zk40004 (at 940 m) and Zk31901 (at 670 m), respectively (Figs. 3, and 6d-i). Zircon grains were separated using heavy liquid and magnetic techniques and then purified by hand picking under a binocular microscope. Approximately 100–200 grains were randomly selected, mounted in epoxy and then polished to about half of their thickness. Internal structures of the zircons were examined using cathodoluminescence (CL) imaging prior to isotopic analysis. Laser ablation ICP-MS zircon U-Pb analyses were conducted on

an Agilent 7500a ICP-MS equipped with a 193 nm laser at the State Key Laboratory of Continental Dynamics, Northwest University, Xian, China, following the method of Yuan et al. (2004). The $^{207}\text{Pb}/^{206}\text{Pb}$ and $^{206}\text{Pb}/^{238}\text{U}$ ratios were calculated using the GLITTER program, which was corrected using the Harvard zircon 91,500 as external calibrant. The detailed analytical technique is described in Yuan et al. (2004). Common Pb contents were therefore evaluated using the method described by Andersen (2002). The age calculations and plotting of concordia diagrams were made using ISOPLOT (version 3.0) (Ludwig, 2003).

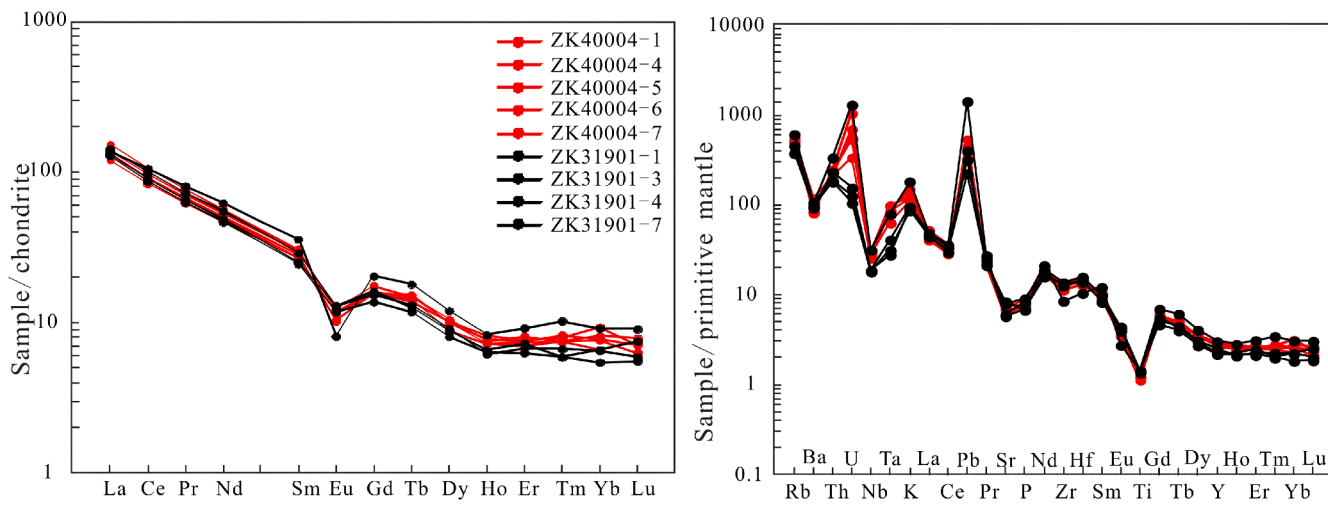


Fig. 9. Chondrite-normalized REE patterns (a) and primitive mantle-normalized incompatible element patterns (b) for the hidden granite. Chondrite-normalized values are from Boynton (1984) and primitive mantle values are from Sun and McDonough (1989).

4.4. Muscovite $^{40}\text{Ar}/^{39}\text{Ar}$ geochronology

The selected muscovite grains were irradiated with neutrons at the TRIGA Reactor of United States Geological Survey, Denver, USA. The total time for irradiation was 48 h; the neutron flux was about $6.0 \times 10^{12}\text{n cm}^{-2}\text{s}^{-1}$; and the integrated neutron flux was $1.13 \times 10^{18}\text{n cm}^{-2}$. A monitor sample, which is an internal standard biotite GA1550 with its age at $99.769 \pm 0.108\text{ Ma}$ (Renne et al., 2010) was also irradiated in the same time with the selected muscovite samples. The stepwise heating was performed on the prepared muscovite grains in an electron impact furnace. The heating extraction steps for each temperature increment lasted 30 min. Mass analysis was performed using VG 5400 Mass Spectrometer at the Arizona Noble Gas Laboratory, University of Arizona, USA. The correction factors of interfering isotopes produced during irradiation were determined by analyzing the irradiated K_2SO_4 and CaF_2 pure salts and their values are: $(^{36}\text{Ar}/^{37}\text{Ar})_{\text{Ca}} = 0.0002389$, $(^{40}\text{Ar}/^{39}\text{Ar})_{\text{K}} = 0.004782$, and $(^{39}\text{Ar}/^{37}\text{Ar})_{\text{Ca}} = 0.000806$. All ^{37}Ar were corrected for radiogenic decay. The ^{40}K decay constant used was $5.543 \times 10^{-10}\text{a}^{-1}$ (Steiger and Jäger, 1977).

4.5. Molybdenite Re-Os ages

The molybdenite samples were crushed in an agate mortar, and then molybdenite grains were handpicked under a binocular microscope to ensure that the purity of more than 99%. The sampled molybdenite was fine-grained (0.1 mm) in order to prevent decoupling of Re and Os within large grains (Selby and Creaser, 2001). Re-Os isotope analysis was performed using an inductively coupled plasma mass spectrometer (ICPMS) in the Isotope Laboratory, Guangzhou Institute of Geochemistry, CAS. The Carius tubes method was used to digest samples (Shirey and Walker, 1995), and Re and Os were separated using the distillation technique described in Du et al. (2004). Details of the chemical procedure were described by Sun et al. (2001, 2010). Molybdenite model ages were calculated using a ^{187}Re decay constant of 1.666×10^{-11} per year, following the equation $t = [\ln(1 + ^{187}\text{Os}/^{187}\text{Re})]/\lambda$, ($\lambda = ^{187}\text{Re}$ decay constant; Smoliar et al., 1996).

4.6. Hf isotopic analyses

After completing the zircon U-Pb dating, the same samples were measured for Hf isotopy. The analyses were conducted using a Neptune Plus multi-collector (MC)-ICP-MS equipped with a RESO lution M-50 laser ablation system at the State Key Laboratory of Isotopic Geochemistry, GIGCAS. The Lu-Hf isotopic measurements were made on

the same spots previously used for the U-Pb analysis. Zircon standard Penglai was used as a reference standard (Li et al., 2010), and the analytical procedures were described by Wu et al. (2006). Initial Hf isotope ratios were calculated using the Chondritic Uniform Reservoir (CHUR) value at the time of zircon crystallization and present-day $^{179}\text{Hf}/^{177}\text{Hf}$ and $^{176}\text{Lu}/^{177}\text{Hf}$ ratios of chondrite and depleted mantle, respectively (Blichert-Toft and Albarede, 1997). Initial $^{176}\text{Hf}/^{177}\text{Hf}$ values were calculated based on a ^{176}Lu decay constant of $1.867 \times 10^{-11}/\text{a}$ (Söderlund et al., 2004), and single-stage model Hf ages (T_{DM1}) were determined with reference to the depleted mantle using a present-day $^{176}\text{Lu}/^{177}\text{Hf}$ ratio of 0.28325 and a $^{176}\text{Lu}/^{177}\text{Hf}$ ratio of 0.0384 (Griffin et al., 2000). Two-stage model Hf ages (T_{DM2}) were computed using the $^{176}\text{Lu}/^{177}\text{Hf}$ value of 0.015 for the average continental crust (Griffin et al., 2002).

5. Results

5.1. Major and trace elemental geochemistry

Results of geochemical analyses of the granite samples are shown in Supplementary Tables 1 and 2. All the samples are plotted in the granite field in the total alkaline-silica (TAS) diagram (Fig. 7a) (Middlemost, 1994), displaying similar chemical composition. They exhibit high contents of SiO_2 (70.09–71.81 wt%), and Al_2O_3 (13.32–14.79 wt%), and low contents of MgO (0.63–0.79 wt%), Fe_2O_3 (1.53–2.84 wt%), and CaO (0.92–2.25 wt%). The samples are characterized by high K_2O (2.61–5.47 wt%), $\text{K}_2\text{O} + \text{Na}_2\text{O}$ (6.87–8.23) and $\text{K}_2\text{O}/\text{Na}_2\text{O}$ ratios (0.58–1.98), showing an affinity to high-K calc-alkaline series (Fig. 7c) (Peccerillo and Taylor, 1976). These samples are strongly peraluminous with A/CNK [molar $\text{Al}_2\text{O}_3/(\text{CaO} + \text{Na}_2\text{O} + \text{K}_2\text{O})$] ranging from 1.50 to 1.61 and A/NK [molar $\text{Al}_2\text{O}_3/(\text{Na}_2\text{O} + \text{K}_2\text{O})$] from 1.62 to 2.08 (Fig. 7b) (Maniar and Piccoli, 1989), similar to the S-type granites as defined by White and Chappell (1977). The CIPW-normative calculation gives 28.25 to 32.47 vol% Qz , 15.56 to 32.78 vol% Or , 23.68 to 38.32 vol% Ab , 3.43 to 9.92 vol% An , and 0.73 to 1.93 vol% corundum. On Harker diagrams (Fig. 8), the MgO , Fe_2O_3 , Na_2O and CaO contents of the granite samples show negative correlations with SiO_2 , whereas TiO_2 , Al_2O_3 and P_2O_5 remain nearly constant. The Xidamingshan hidden granite has high DI values (82.13–88.93), suggesting that it has experienced a significant magmatic differentiation. The granite samples from both drill holes display similar chemical compositions, characterized by low TiO_2 (0.25–0.32 wt%) and P_2O_5 (0.15–0.20 wt%), suggesting fractional crystallization of ferromagnesian minerals (biotite and/or hornblende), Ti-Fe oxides, and apatite.

Table 3

Analytical data of zircon LA-ICP-MS U-Pb dating for sample Zk40004-1.

Sample No.	Th ppm	U ppm	Th/U	Isotopic ratio								Age (Ma)							
				$\frac{^{207}\text{Pb}}{^{206}\text{Pb}}$	1σ	$\frac{^{207}\text{Pb}}{^{235}\text{U}}$	1σ	$\frac{^{206}\text{Pb}}{^{238}\text{U}}$	1σ	$\frac{^{208}\text{Pb}}{^{232}\text{Th}}$	1σ	$\frac{^{207}\text{Pb}}{^{206}\text{Pb}}$	1σ	$\frac{^{207}\text{Pb}}{^{235}\text{U}}$	1σ	$\frac{^{206}\text{Pb}}{^{238}\text{U}}$	1σ	$\frac{^{208}\text{Pb}}{^{232}\text{Th}}$	1σ
ZK40004-1-01	41.8	1859.8	0.02	0.0456	0.0021	0.1035	0.0036	0.0165	0.0003	0.0068	0.0005	0.1	79.2	100.0	3.3	105.4	1.6	137.6	10.3
ZK40004-1-04	77.0	1487.6	0.05	0.0481	0.0020	0.1073	0.0032	0.0162	0.0002	0.0048	0.0002	103.3	94.5	103.5	2.9	103.5	1.5	96.7	4.7
ZK40004-1-06	1041.1	2649.0	0.39	0.0519	0.0020	0.1108	0.0028	0.0155	0.0002	0.0050	0.0001	279.9	84.9	106.7	2.5	99.1	1.4	101.0	1.8
ZK40004-1-07	307.8	771.8	0.4	0.0498	0.0024	0.1066	0.0041	0.0155	0.0002	0.0045	0.0001	185.6	108.3	102.8	3.7	99.3	1.5	91.3	2.2
ZK40004-1-08	214.3	2980.8	0.07	0.0477	0.0018	0.1039	0.0025	0.0158	0.0002	0.0044	0.0001	85.7	87.9	100.4	2.3	100.9	1.4	89.3	2.9
ZK40004-1-09	179.4	2494.9	0.07	0.0491	0.0021	0.1052	0.0033	0.0156	0.0002	0.0053	0.0002	151.7	97.8	101.6	3.1	99.5	1.5	106.6	4.4
ZK40004-1-10	328.4	2308.7	0.14	0.0485	0.0020	0.1045	0.0031	0.0156	0.0002	0.0043	0.0001	122.3	94.1	100.9	2.8	100.0	1.5	87.0	2.6
ZK40004-1-11	200.2	1653.7	0.12	0.0487	0.0022	0.1045	0.0035	0.0156	0.0002	0.0051	0.0002	130.9	101.8	100.9	3.3	99.6	1.5	102.3	3.6
ZK40004-1-12	339.3	3148.6	0.11	0.0482	0.0018	0.1034	0.0023	0.0156	0.0002	0.0053	0.0001	111.0	84.0	99.9	2.2	99.5	1.4	106.5	2.4
ZK40004-1-14	232.2	1449.3	0.16	0.0492	0.0022	0.1058	0.0037	0.0156	0.0002	0.0042	0.0002	156.8	103.2	102.1	3.4	99.8	1.5	84.6	3.0
ZK40004-1-15	1848.2	1255.6	1.47	0.0525	0.0023	0.1118	0.0036	0.0154	0.0002	0.0047	0.0001	307.3	95.4	107.6	3.3	98.7	1.5	95.1	1.4
ZK40004-1-16	303.6	3112.5	0.1	0.0475	0.0017	0.1021	0.0023	0.0156	0.0002	0.0056	0.0001	75.3	84.9	98.7	2.1	99.6	1.4	113.3	2.6
ZK40004-1-17	370.9	2868.0	0.13	0.0473	0.0018	0.1021	0.0026	0.0157	0.0002	0.0046	0.0001	61.6	90.1	98.7	2.4	100.2	1.4	93.2	2.4
ZK40004-1-18	719.1	3182.7	0.23	0.0471	0.0019	0.1022	0.0028	0.0157	0.0002	0.0043	0.0001	56.0	93.4	98.8	2.6	100.6	1.4	86.9	2.0
ZK40004-1-19	141.6	440.0	0.32	0.0480	0.0038	0.0996	0.0073	0.0150	0.0003	0.0050	0.0002	101.4	177.6	96.4	6.7	96.2	1.9	100.0	4.5
ZK40004-1-20	129.1	546.5	0.24	0.0508	0.0036	0.1074	0.0067	0.0153	0.0003	0.0046	0.0002	230.8	154.0	103.6	6.2	98.1	1.8	92.2	4.7
ZK40004-1-21	121.6	2628.7	0.05	0.0474	0.0018	0.1025	0.0025	0.0157	0.0002	0.0048	0.0002	67.8	87.3	99.1	2.3	100.4	1.4	97.4	3.7
ZK40004-1-22	554.8	1396.2	0.4	0.0500	0.0021	0.1142	0.0036	0.0166	0.0003	0.0046	0.0001	193.7	96.6	109.8	3.3	106.0	1.6	91.7	2.0
ZK40004-1-23	226.9	736.7	0.31	0.0466	0.0024	0.0989	0.0042	0.0154	0.0002	0.0048	0.0001	29.4	119.1	95.8	3.9	98.4	1.5	97.2	2.8
ZK40004-1-24	103.0	4204.2	0.02	0.0527	0.0019	0.1081	0.0023	0.0149	0.0002	0.0113	0.0003	314.3	79.1	104.2	2.1	95.2	1.3	227.9	6.4
ZK40004-1-25	232.4	459.6	0.51	0.0478	0.0035	0.0999	0.0066	0.0152	0.0003	0.0043	0.0002	89.7	165.3	96.7	6.1	96.9	1.8	86.1	3.0
ZK40004-1-26	374.4	3568.7	0.1	0.0495	0.0018	0.1066	0.0024	0.0156	0.0002	0.0044	0.0001	172.4	83.5	102.9	2.2	99.8	1.4	89.4	2.2
ZK40004-1-27	254.2	4343.0	0.06	0.0516	0.0018	0.1112	0.0023	0.0156	0.0002	0.0068	0.0002	267.3	79.1	107.0	2.1	99.9	1.4	136.3	3.2
ZK40004-1-28	283.2	1634.0	0.17	0.0499	0.0020	0.1073	0.0029	0.0156	0.0002	0.0047	0.0001	188.5	90.0	103.5	2.7	99.8	1.4	93.8	2.3
ZK40004-1-29	683.3	1769.7	0.39	0.0520	0.0024	0.1110	0.0039	0.0155	0.0002	0.0044	0.0001	286.1	101.1	106.9	3.5	99.0	1.5	88.6	2.1
ZK40004-1-30	325.7	2341.3	0.14	0.0489	0.0019	0.1054	0.0027	0.0156	0.0002	0.0042	0.0001	143.4	88.5	101.7	2.5	99.9	1.4	85.3	2.3

Table 4
Analytical data of zircon LA-ICP-MS U-Pb dating for sample ZK31901-1.

Sample No.	Th ppm	U ppm	Th/U	Isotopic ratio				Age (Ma)			
				$\frac{^{207}\text{Pb}}{^{206}\text{Pb}}$		$\frac{^{207}\text{Pb}}{^{235}\text{U}}$		$\frac{^{206}\text{Pb}}{^{238}\text{U}}$		$\frac{^{207}\text{Pb}}{^{235}\text{U}}$	
				1σ	1σ	1σ	1σ	1σ	1σ	1σ	1σ
ZK31901-1-01	389.6	2466.3	0.16	0.0480	0.0015	0.1001	0.0029	0.0151	0.0001	0.0052	0.0001
ZK31901-1-02	1198.2	754.1	1.59	0.0522	0.0035	0.1091	0.0071	0.0152	0.0002	0.0048	0.0001
ZK31901-1-03	2665.8	2302.8	1.16	0.0506	0.0024	0.1051	0.0048	0.0151	0.0002	0.0043	0.0001
ZK31901-1-04	579.1	3441.3	0.17	0.0487	0.0014	0.1027	0.0027	0.0153	0.0001	0.0038	0.0001
ZK31901-1-05	1229.0	1913.4	0.64	0.0462	0.0018	0.0974	0.0036	0.0153	0.0001	0.0045	0.0001
ZK31901-1-07	1018.5	1210.5	0.84	0.0488	0.0030	0.1015	0.0060	0.0151	0.0002	0.0048	0.0001
ZK31901-1-10	3179.9	2795.1	1.14	0.0522	0.0020	0.1068	0.0038	0.0149	0.0001	0.0048	0.0001
ZK31901-1-11	661.5	3805.9	0.17	0.0472	0.0014	0.1015	0.0029	0.0156	0.0001	0.0043	0.0001
ZK31901-1-12	368.0	5216.4	0.07	0.0475	0.0012	0.1019	0.0022	0.0155	0.0001	0.0042	0.0002
ZK31901-1-17	3522.7	2906.2	0.14	0.0468	0.0015	0.0980	0.0030	0.0152	0.0001	0.0046	0.0002
ZK31901-1-18	3574.0	2049.9	1.74	0.0518	0.0026	0.1073	0.0052	0.0150	0.0001	0.0049	0.0001
ZK31901-1-22	1620.1	2690.7	0.6	0.0481	0.0018	0.1058	0.0038	0.0160	0.0001	0.0045	0.0001
ZK31901-1-23	857.7	1944.1	0.44	0.0483	0.0020	0.1043	0.0041	0.0157	0.0001	0.0052	0.0001
ZK31901-1-24	261.8	347.1	0.75	0.0503	0.0056	0.1074	0.0118	0.0155	0.0003	0.0046	0.0002
ZK31901-1-25	564.3	2180.9	0.26	0.0450	0.0025	0.0922	0.0051	0.0149	0.0002	0.0046	0.0002
ZK31901-1-28	1598.0	1831.6	0.87	0.0505	0.0021	0.1057	0.0041	0.0152	0.0001	0.0042	0.0001
ZK31901-1-29	1288.6	3575.8	0.36	0.0497	0.0017	0.1077	0.0034	0.0157	0.0001	0.0047	0.0001

The granite contains relatively low total REE concentrations ($\Sigma\text{REE} = 128.08 - 151.79$ ppm with an average of 134.92 ppm), with LREE/HREE ratios of 11.55 – 14.57. In the chondrite-normalized REE diagram (Fig. 9a) (Sun and McDonough, 1989), the granite samples show enrichment in light REE and are characterized by a right-inclined shape. The granite samples have significant LREE/HREE fractionation with $(\text{La/Yb})_N$ ratios of 15.23 – 23.38 and weak negative Eu anomalies ($\text{Eu}/\text{Eu}^* = 0.29 - 0.63$), which is a typical characteristics of moderately evolved magmas. Normalized to primitive mantle (Fig. 9b) (Sun and McDonough, 1989), all the samples of the Xidamingshan hidden granite exhibit similar trace elemental patterns, with significant negative anomalies of high field strength elements (e.g., Nb, Ti and P) and positive anomalies of large-ion lithophile elements (e.g., Rb, Ta, Th, U and K). Magmas of such granite could have fractionally crystallized LREE-rich minerals such as biotite, feldspar and apatite.

5.2. U-Pb zircon age

Tables 3 and 4 show isotopic data obtained from the LA-ICP-MS U-Pb zircon analysis for samples ZK40004-1 and ZK31901-1, respectively. The zircon grains are transparent, euhedral and prismatic crystals with elongation ratios ranging from 1 to 3 μm and diameters from 50 to 250 μm . Some zircon grains have growth preference in certain orientations, resulting in exterior imperfections (Fig. 10). CL images exhibit strong oscillatory zoning with variable luminescence. Most of the Th/U ratios are greater than 0.1, indicating typical magmatic origin (Williams et al., 1996; Rubatto and Gebauer, 2000).

For the sample ZK40004-1, twenty-six zircon grains were analyzed. They have Th concentrations ranging from 41.84 to 1848.2 ppm, U content between 440.0 and 4343.0 ppm and Th/U ratios in the range of 0.02 – 1.47 (Table 3). Twenty-six spots yielded a coherent cluster with the $^{206}\text{Pb}/^{238}\text{U}$ weighted mean age of 99.8 ± 0.9 Ma (MSWD = 2.3) (Fig. 11a). For the sample ZK31901-1, seventeen zircon grains were analyzed. Their Th and U concentrations range from 261.8 to 3574.0 ppm and 347.1 to 5216.4 ppm, respectively, with Th/U ratios mostly in the range of 0.07 to 1.74 (Table 4). The analysis yielded a $^{206}\text{Pb}/^{238}\text{U}$ weighted mean age of 98.0 ± 1.0 Ma (MSWD = 4.9) (Fig. 11b).

5.3. Ar-Ar muscovite age

The results of Ar-Ar analyses of hydrothermal muscovite samples ZK31901-10 and ZK31901-10i are presented in Table 5 and the corresponding plateau age are plotted in Fig. 12a and 12b, respectively. Muscovite from sample ZK31901-10 was incrementally heated with 11 steps from 600 °C to 1050 °C, which yielded a concordant age spectrum. The plateau comprises 6 continuous steps accounting for 90% of the released total $^{39}\text{Ar}_\text{K}$, indicating that K and radiogenic ^{40}Ar in the sample are distributed homogeneously, and that K-Ar isotopic systematics was not affected by heating disturbances over the geological history of the sample (Liu et al., 2017). Plateau age was determined using the criteria of Dalrymple and Lanphere (1971). It yielded a plateau age of 93 ± 3 Ma (Fig. 12a). Muscovite from sample ZK31901-10i was incrementally heated with 6 steps from 875 °C to 1,100 °C (Fig. 12b). Five continuous steps at temperature of 925 – 1100 °C are relatively coincident, constituting a uniform and distinctly flat $^{40}\text{Ar}/^{39}\text{Ar}$ age spectra with 100% ^{39}Ar released. These steps yielded a well-defined plateau age of 92 ± 3 Ma. This plateau age of the muscovite sample is almost identical with that of the sample ZK31901-10 within analytical error. Therefore, the $^{40}\text{Ar}/^{36}\text{Ar}$ ages of the sample are considered to be reliable. The coincident plateau age can be used to estimate the crystallization age of muscovite after systematic error corrections.

5.4. Re-Os molybdenite ages

Table 6 and Fig. 13 show that these samples display a relatively low Re content, ranging from 1.9824 to 13.8546 ppm, ^{187}Re content is

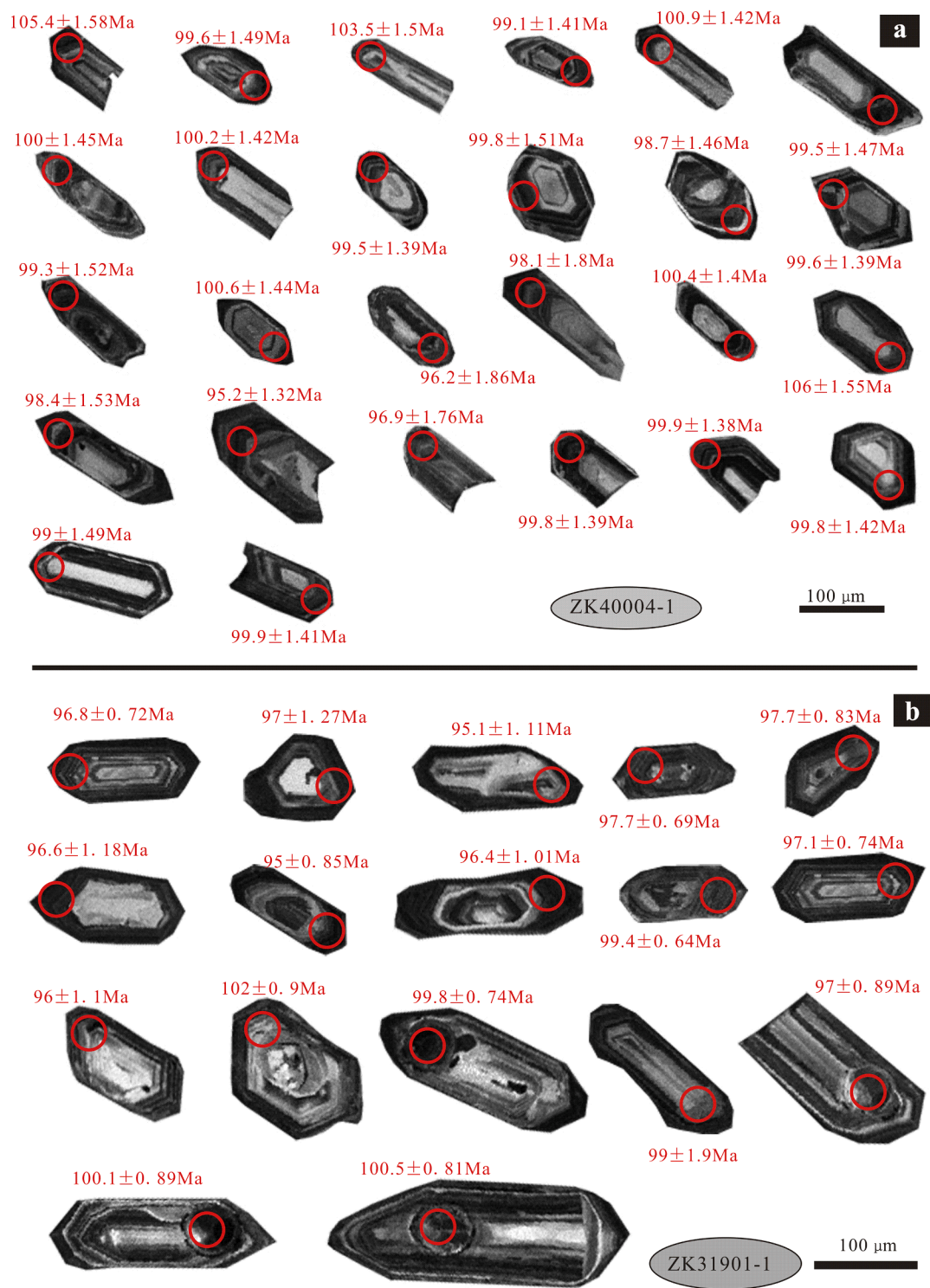


Fig. 10. Cathodoluminescence (CL) images of zircon grains selected from the biotite granite samples Zk40004-1 (A) and ZK31901-1 (B) at Luowei deposit.

between 1.246 and 8.7081 ppm and ^{187}Os content is between 1.9137 and 13.8524 ppb. The Re-Os isochron and average weighted ages were calculated using the ISOPLOT program (Ludwig, 2003). The analyzed samples yielded model ages ranging from 92.1 ± 1.0 Ma to 95.7 ± 0.3 Ma, with a well-constrained ^{187}Re - ^{187}Os isochron age of 95.9 ± 1.7 Ma (MSWD = 2.2) (Fig. 13a), and a weighted mean age of 95.0 ± 0.3 Ma (MSWD = 3.1) (Fig. 13b). The isochron age is consistent well with the weighted mean age, conforming that the molybdenite contains no

detectable common ^{187}Os (initial $^{187}\text{Os}/^{188}\text{Os} = -0.09 \pm 0.16$) and that the molybdenite Re-Os dating is reliable.

5.5. *Hf isotopes*

The Hf isotopic results of zircons are given in Table 7 and graphically presented in Figs. 14 and 15. Forty-two spot analyses were obtained from 42 grains of Sample ZK40004-1 and ZK31901-1. The $^{176}\text{Lu}/^{177}\text{Hf}$

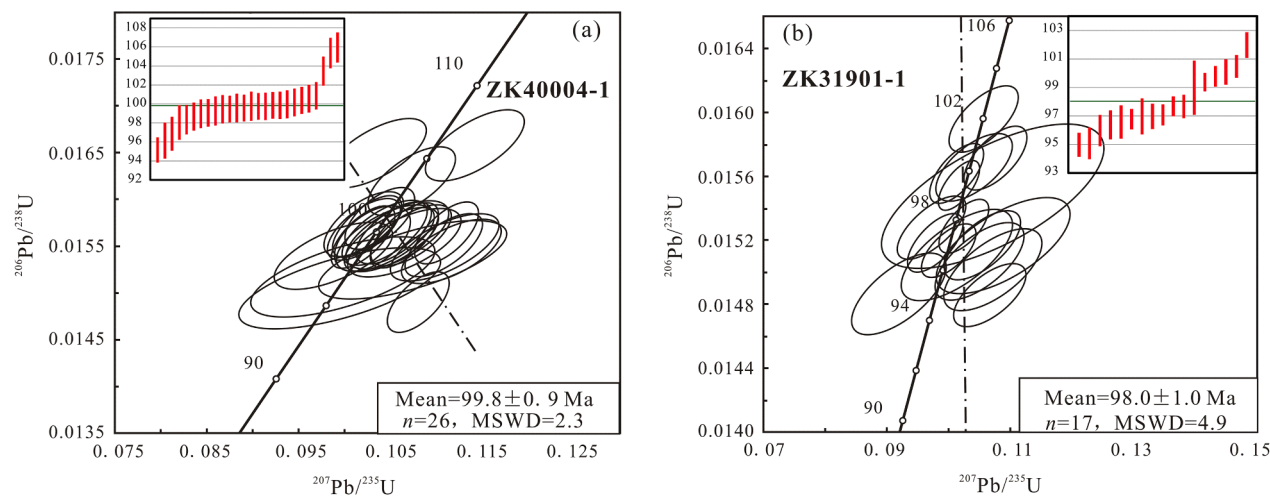


Fig. 11. Zircon U-Pb concordia and weighted mean ages of the samples Zk40004-1 and ZK31901-1.

Table 5

$^{40}\text{Ar}/^{39}\text{Ar}$ analytical data for muscovite from samples ZK31901-10i and ZK31901-10.

ZK31901-10									
Heating step	T(°C)	$^{40}\text{Ar}/^{39}\text{Ar}$	$^{37}\text{Ar}/^{39}\text{Ar}$	$^{36}\text{Ar}/^{39}\text{Ar} (\times 10^{-3})$	$^{39}\text{Ar}_K(\times 10^{-16} \text{ mol})$	$^{40}\text{Ar}^*(\%)$	$^{39}\text{Ar}(\%)$	Apparent age (Ma)	$\pm 1\text{s} (\text{Ma})$
B	600	100.98	-118.232	-0.0562	0.1172	107.20	0.46	204.8	71.5
C	625	135.77	-5.013	-0.0072	0.1432	101.27	0.57	275.1	62.3
D	650	95.44	-20.840	0.0430	0.3376	84.80	1.34	165.2	25.6
E	675	66.10	-5.998	0.0451	1.9305	78.91	7.64	109.3	4.6
F	700	54.85	-8.326	0.0192	1.5309	88.30	6.06	101.5	5.8
G	750	51.98	-2.052	0.0273	4.1090	84.02	16.27	92.2	2.2
H	800	51.07	-0.681	0.0203	6.0768	88.00	24.06	94.9	1.5
I	900	50.19	-4.751	0.0187	7.1840	88.10	28.44	93.1	1.3
J	950	48.06	-1.674	0.0301	1.3567	81.04	5.37	82.5	6.8
K	1000	47.92	-0.403	0.0262	1.4615	83.64	5.79	84.9	6.4
L	1050	43.69	-1.608	0.0201	1.0144	85.93	4.02	79.6	9.2
ZK31901-10i									
K	875	49.31	0.410	0.0185	4.1087	88.87	43.08	92.7	1.4
M	925	48.45	1.425	0.0274	0.8734	83.34	9.16	85.6	7.0
N	950	47.47	-0.452	0.0254	0.6966	83.94	7.30	84.4	8.9
O	1000	47.74	0.651	0.0269	0.8178	83.30	8.57	84.3	7.5
P	1050	46.64	0.957	0.0116	2.4068	92.76	25.23	91.5	2.6
Q	1100	46.46	-0.671	0.0184	0.6346	88.05	6.65	86.6	9.8

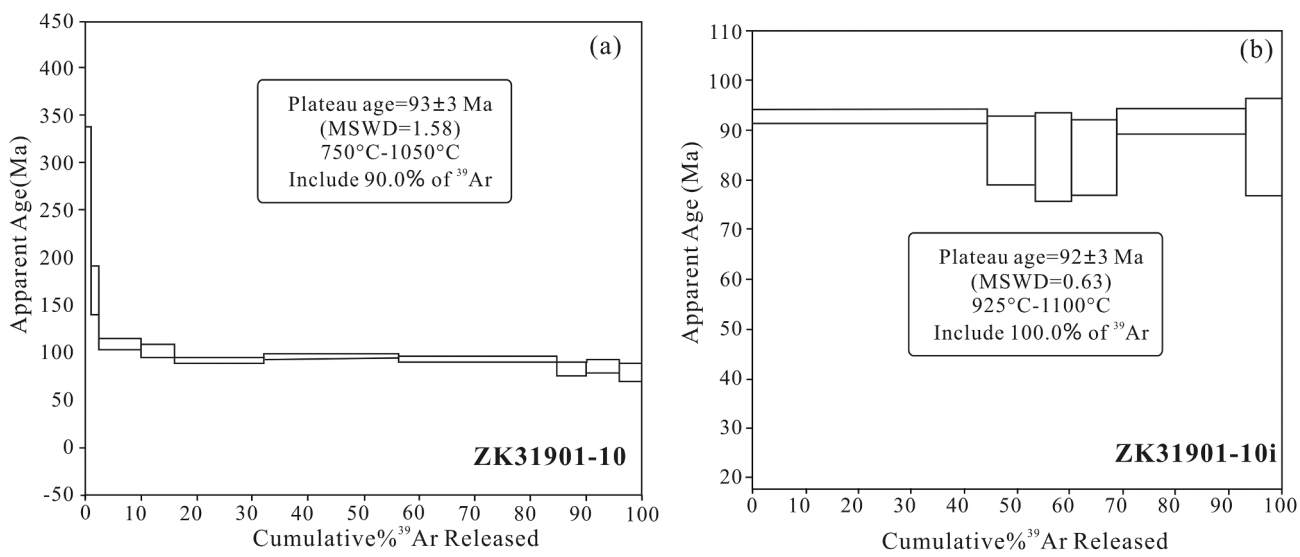


Fig. 12. Muscovite $^{40}\text{Ar}-^{39}\text{Ar}$ plateau age of samples ZK31901-10 and ZK31901-10i.

Table 6

Re–Os isotope composition of molybdenites from the Xidamingshan district.

Sample no.	Weight(g)	Re (ppm)		^{187}Re (ppm)		^{187}Os (ppb)		Model age (Ma)	
		Measured	2σ	Measured	2σ	Measured	2σ	Measured	2σ
ZK40004-15	0.0625	8.3827	0.039	5.2689	0.0245	8.3652	0.0338	95.2	0.6
ZK40004-15	0.0624	7.8676	0.0374	4.9451	0.0235	7.699	0.0365	93.4	0.6
ZK40004-16	0.0561	8.5303	0.0272	5.3616	0.0171	8.5582	0.0015	95.7	0.3
ZK40004-16	0.0319	8.4084	0.0157	5.285	0.0099	8.3805	0.0061	95.1	0.2
ZK40004-17	0.0632	8.6879	0.0229	5.4607	0.0144	8.5683	0.0436	94.1	0.5
ZK41602-1	0.0314	13.8546	0.0931	8.7081	0.0585	13.8524	0.0733	95.4	0.8
ZK41602-7	0.0317	8.1199	0.0261	5.1037	0.0164	8.1123	0.0866	95.3	1.1
ZK41602-13	0.0303	8.6211	0.0433	5.4187	0.0272	8.5405	0.0609	94.5	0.8
ZK41602-14	0.0204	1.9824	0.0068	1.246	0.0043	1.9137	0.0195	92.1	1.0

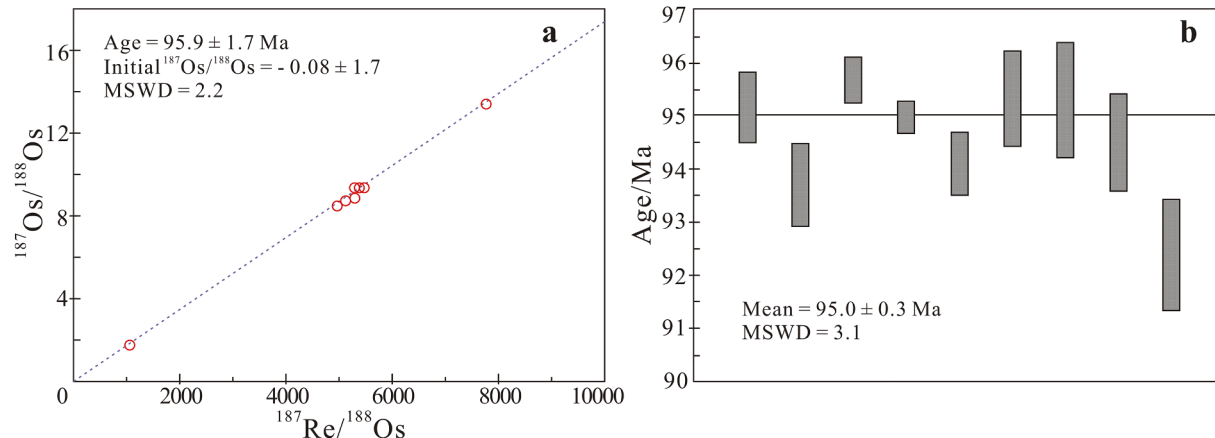


Fig. 13. Re–Os isochron plot for molybdenite samples from the Luowei deposit.

ratios of most zircon grains are lower than 0.0025, suggesting that the zircon grains have accumulated little radiogenic Hf after they formed. Therefore, the $^{176}\text{Hf}/^{177}\text{Hf}$ ratios represent the isotopic composition of the zircons when they were crystallized (Patchett et al., 1981; Knudsen et al., 2001; Kinny and Maas, 2003). The Hf isotopic analyses for zircon grains from the two hidden pluton samples (ZK40004-1 and ZK31901-1) show the homogeneous Hf isotopic compositions, with initial $^{176}\text{Hf}/^{177}\text{Hf}$ ratios of 0.282358 – 0.282574 and 0.282388 – 0.282647 and calculated $\varepsilon_{\text{Hf}}(t)$ values in the range of –4.9 to –12.6 (average value of –8.0) and –2.4 to –11.5 (average value of –7.2), respectively (Fig. 14), corresponding to two-stage model ages (T_{DM2}) of 1476 – 1964 Ma and 1316 – 1893 Ma, respectively.

6. Discussion

6.1. Timing of the granitic emplacement and mineralization

Very few studies on geochronology have been carried out for the Xidamingshan district. High-precision zircon U-Pb geochronological method can provide reliable magmatic emplacement age, since the closure temperature of the U-Pb isotopic system within zircon (estimated at about $700 \pm 50^\circ\text{C}$) is comparable with that of crystallization in granitic plutons (Dodson and McClelland-Brown, 1985). In this study, two samples of the Xidamingshan hidden granite pluton from different drilling holes yielded similar zircon U-Pb ages (99.8 ± 0.9 Ma and 98.0 ± 1.0 Ma), indicating that the Xidamingshan hidden granitic pluton was emplaced at the Late Cretaceous time. Late Mesozoic granites with an age range of 100 – 80 Ma are widely distributed in South China (e.g., Wu et al., 1984; Wang et al., 2004; Cai et al., 2006; Tan et al., 2008; Chen et al., 2009; Luo et al., 2009; Liu et al., 2010; Feng et al., 2011), and include the Longtoushan rhyolitic porphyry (103 – 100 Ma; Chen et al., 2008), Sheshan granitic complex (91.05 ± 0.31 Ma, Chen et al., 2011),

Maanshan and Zhougongding rhyolitic dacite (100 ± 1 Ma), Deqing monzogranite (99 ± 2 Ma), Xinhua granodiorite (100 Ma) and Tiaocun granodiorite (104 ± 3 Ma) (Geng et al., 2006). Therefore, the geochronological data obtained from this study confirms that the emplacement of the Xidamingshan granite pluton was part of the large-scale Late Yanshanian magmatic province in the interior of South China block. The muscovite $^{40}\text{Ar}-^{39}\text{Ar}$ ages 93 ± 3 Ma and 92 ± 3 Ma (Fig. 12a, b; both are within error range) for the greisen alteration veins are slightly younger (about 7 m.y.r younger) than the zircon U-Pb age, but are similar to the ages reported by previous U-Pb dating work (92.92 ± 0.69 Ma and 92.5 ± 1.1 Ma, Xiao et al., 2018a). Given that the sampled muscovite is of hydrothermal alteration origin (Fig. 3b and 6b), the 92 – 93 Ma ages may represent the latest episode of post-magmatic hydrothermal metallogenetic activity. It is, therefore, suggested that the Xidamingshan granite pluton has experienced a prolonged magmatic emplacement and post-emplacement hydrothermal alteration history.

The Re–Os chronometer in molybdenite is remarkably robust (Stein et al., 2001), and is not easily disturbed by hydrothermal activity (Selby and Creaser, 2001), or by later tectonothermal events (Stein et al., 1998). In general, Re–Os dating of molybdenite provides precise ages for hydrothermal ore deposits. In this study, molybdenite from the Luowei deposit is fine grained, so decoupling of Re and Os is unlikely and Re–Os age data obtained during this study is considered reliable (Selby et al., 2002). The model Re–Os ages of these eight samples ranging from 92.1 ± 1.0 Ma to 95.7 ± 0.3 Ma, and the Re–Os isochron age (95.9 ± 1.7 Ma) of the molybdenite samples represent the timing of Luowei mineralization at the Xidamingshan district, because the molybdenite is intergrown with wolframite. We infer from these ages that the mineralization in the Xidamingshan mining district occurred during the emplacement of the Xidamingshan biotite granite pluton, coeval with the development of skarn at the contact with the pluton and the presence of greisen on the top of the pluton.

Table 7
Zircon Hf isotopic data.

Sample No.	$^{176}\text{Lu}/^{177}\text{Hf}$	$^{176}\text{Hf}/^{177}\text{Hf}$	2σ	Age(Ma)	$t_{\text{DM1}}(\text{Ma})$	$t_{\text{DM2}}(\text{Ma})$	$\varepsilon_{\text{Hf}}(t)$	2σ
ZK40004-1-1	0.000996	0.282531	0.000022	99.8	1021	1570	-6.4	0.8
ZK40004-1-4	0.001695	0.282563	0.000020	99.8	994	1501	-5.3	0.7
ZK40004-1-6	0.002196	0.282503	0.000023	99.8	1095	1637	-7.5	0.8
ZK40004-1-7	0.003625	0.282481	0.000033	99.8	1173	1692	-8.3	1.2
ZK40004-1-8	0.002148	0.282520	0.000024	99.8	1069	1599	-6.9	0.8
ZK40004-1-9	0.002811	0.282358	0.000026	99.8	1327	1964	-12.6	0.9
ZK40004-1-10	0.001482	0.282564	0.000019	99.8	987	1498	-5.3	0.7
ZK40004-1-11	0.001877	0.282500	0.000020	99.8	1090	1643	-7.6	0.7
ZK40004-1-14	0.002009	0.282495	0.000023	99.8	1101	1655	-7.7	0.8
ZK40004-1-15	0.001927	0.282526	0.000028	99.8	1054	1585	-6.6	1.0
ZK40004-1-16	0.002229	0.282498	0.000020	99.8	1103	1649	-7.7	0.7
ZK40004-1-17	0.001571	0.282498	0.000020	99.8	1084	1646	-7.6	0.7
ZK40004-1-18	0.001835	0.282469	0.000018	99.8	1133	1712	-8.7	0.6
ZK40004-1-19	0.000920	0.282415	0.000026	99.8	1181	1830	-10.5	0.9
ZK40004-1-20	0.000651	0.282494	0.000020	99.8	1063	1652	-7.7	0.7
ZK40004-1-21	0.002417	0.282473	0.000022	99.8	1146	1706	-8.5	0.8
ZK40004-1-22	0.001720	0.282574	0.000022	99.8	979	1476	-4.9	0.8
ZK40004-1-23	0.001302	0.282525	0.000019	99.8	1038	1585	-6.6	0.7
ZK40004-1-24	0.003234	0.282456	0.000027	99.8	1197	1747	-9.2	1.0
ZK40004-1-25	0.002020	0.282439	0.000026	99.8	1182	1780	-9.7	0.9
ZK40004-1-26	0.003168	0.282436	0.000023	99.8	1225	1791	-9.9	0.8
ZK40004-1-27	0.002810	0.282430	0.000023	99.8	1221	1803	-10.1	0.8
ZK40004-1-28	0.002953	0.282454	0.000024	99.8	1191	1750	-9.3	0.8
ZK40004-1-29	0.002494	0.282527	0.000024	99.8	1069	1585	-6.6	0.8
ZK40004-1-30	0.002514	0.282449	0.000030	99.8	1184	1760	-9.4	1.1
ZK31901-1-1	0.002368	0.282647	0.000025	98	890	1316	-2.4	0.9
ZK31901-1-2	0.002001	0.282573	0.000028	98	988	1481	-5.0	1.0
ZK31901-1-3	0.001936	0.282489	0.000025	98	1108	1669	-8.0	0.9
ZK31901-1-4	0.001609	0.282494	0.000024	98	1091	1656	-7.8	0.8
ZK31901-1-5	0.002093	0.282542	0.000026	98	1036	1551	-6.1	0.9
ZK31901-1-7	0.001525	0.282536	0.000026	98	1028	1562	-6.3	0.9
ZK31901-1-10	0.001252	0.282515	0.000025	98	1051	1608	-7.0	0.9
ZK31901-1-11	0.002099	0.282461	0.000026	98	1153	1732	-9.0	0.9
ZK31901-1-12	0.002178	0.282410	0.000022	98	1229	1847	-10.8	0.8
ZK31901-1-17	0.001174	0.282499	0.000025	98	1071	1644	-7.6	0.9
ZK31901-1-18	0.002415	0.282559	0.000026	98	1020	1514	-5.5	0.9
ZK31901-1-22	0.001516	0.282516	0.000019	98	1057	1607	-7.0	0.7
ZK31901-1-23	0.001537	0.282512	0.000024	98	1063	1616	-7.1	0.8
ZK31901-1-24	0.000822	0.282598	0.000024	98	922	1420	-4.1	0.8
ZK31901-1-25	0.001419	0.282388	0.000024	98	1235	1893	-11.5	0.8
ZK31901-1-28	0.002112	0.282469	0.000027	98	1142	1714	-8.7	1.0
ZK31901-1-29	0.001887	0.282494	0.000023	98	1099	1657	-7.8	0.8

6.2. Petrogenesis and source of the granitic magmas

Traditionally, granites have been divided into I, S, M and A types based on their geochemical characteristics (Chappell and White, 1974). The main signatures of S type granites are A/CNK greater than 1.1 and the general presence of aluminous primary minerals, such as muscovite, cordierite, tourmaline and garnet (Huang et al., 2017b). As for the genetic type of the Xidamingshan hidden granite pluton, our litho-geochemical and isotopic data indicate that it possess many similarities to the properties of the S-type granite according to traditional granite genetic classification (Chappell and White, 1974; Collins et al., 1982; Pircher, 1983; Wolf and London, 1994; Li et al., 2007a; 2007b), with SiO₂ contents in a range of 70.09 – 71.81 wt% and A/CNK ratios in a range of 1.5 – 1.61. Moreover, the hidden granite pluton contains aluminous primary minerals such as muscovite, biotite, and tourmaline, and the absence of hornblende and riebeckite or other alkaline-rich ferromagnesian minerals also indicate S-type and/or highly fractionated I-type affinity (Chappell and White, 1992). However, the P₂O₅ content of the Xidamingshan hidden granite ranges from 0.15% to 0.20% and remains the similar values with increasing SiO₂ (Fig. 8), which is an indicative of geochemical signature corresponding to the S-type granite but different from the I-type granite (Chappell, 1999; Wu et al., 2003; Li et al., 2006; 2007a; 2007b). On the (Al₂O₃-(Na₂O + K₂O)-CaO-(FeO^T + MgO) diagram (Fig. 7d), these samples are plotted within the plagioclase-muscovite-cordierite field (Hine et al., 1978), suggesting that the plutons are typical S- type granitoids. This

conclusion is further supported by Rb/Sr ratios of 1.33 – 3.12, because for S-type granite, its Rb/Sr ratio is normally greater than 0.9 (e.g., Wang et al., 1993). In addition, the calculated zirconium saturation temperature of the samples is 705 – 783 °C (with an average of 767 °C), which is also close to that of S-type granite (764 °C, King et al., 1997).

The Lu-Hf geochronometer is one of the useful isotopic systems for evaluating magma source of the granitic rocks (Cimen et al., 2018). New zircon Hf isotopic data of the granite samples of the Xidamingshan hidden granite are characterized by $\varepsilon_{\text{Hf}}(t)$ values ranging from -4.9 to -12.6. In the $\varepsilon_{\text{Hf}}(t)$ vs. t diagram (Fig. 15), the data are located predominately below the evolution line of chondrite, along the evolution array of the lower continent, indicating involvement of significant amount of material derived from an enriched and evolved continental source. In addition, the zircon two-stage model ages (T_{DM2}) of 1.31 to 1.96 Ga suggest contributions from evolved Paleoproterozoic to Mesoproterozoic sources. Moreover, the Xidamingshan hidden granite has CaO/Na₂O ratios falling in the field of strongly peraluminous granites (Fig. 16a). Previous studies suggest that partial melting of metasedimentary protoliths including clay-rich metapelites and clay-poor meta-greywackes (psammites) can produce strong peraluminous granitoids (Sylvester, 1998; Clemens, 2003; Zhu et al., 2018). Also, the CaO/Na₂O ratios (less than 0.3) of peraluminous granitic rocks sourced from plagioclase-poor, clay-rich pelitic rocks are distinctly lower than those of granites (>0.3) generated from plagioclase-rich, clay-poor psammitic rocks or meta-igneous rocks (Sylvester, 1998). In the Rb/Sr vs. CaO/Na₂O diagram (Fig. 16b), the samples plot in the plagioclase-rich field

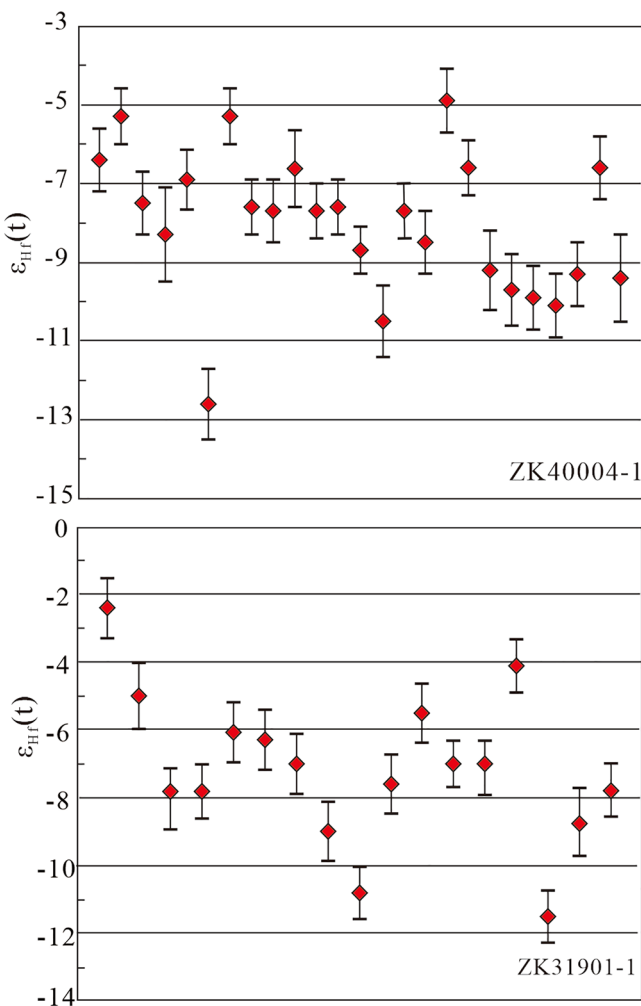


Fig. 14. Distribution diagram of $\epsilon_{\text{Hf}}(t)$ values for the hidden granite pluton.

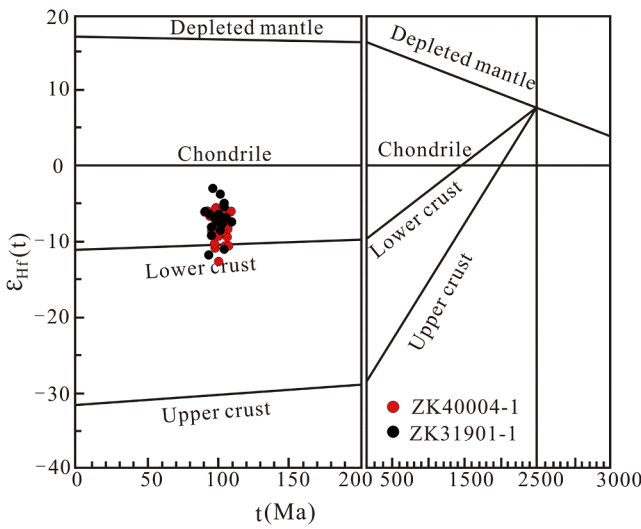


Fig. 15. $\epsilon_{\text{Hf}}(t)$ vs. t diagram of the Xidamingshan hidden granite.

with $\text{CaO}/\text{Na}_2\text{O}$ values of 0.33 – 0.50. In addition, the majority of the samples fall in the clay poor field in the Rb/Sr vs. Rb/Ba discrimination diagram (Fig. 16c) (Sylvester, 1998), and near the shale and sandy fields, displaying obvious affinity to melts derived from clay-poor rocks.

Besides, the Xidamingshan hidden granite is also characterized by low molar $\text{CaO}/(\text{MgO} + \text{FeO}^{\text{T}})$ ratios, with the molar $\text{Al}_2\text{O}_3/(\text{MgO} + \text{FeO}^{\text{T}})$ ratios mostly located in the field of metapelitic-derived melts (Fig. 16d). Taking all the above geochemical data into account, we propose that the Xidamingshan granitic magmas were sourced predominantly from argillaceous-depleted sedimentary rocks. Based on the above discussions, we propose that the Xidamingshan hidden granite is a S-type granite generated by partial melting of crustal materials with argillaceous-depleted sedimentary rocks.

6.3. Associations with W-Zn-Pb-Ag mineralization

A number of mineral deposits have been discovered in the Cambrian strata overlying the Xidamingshan hidden granite pluton, including skarn-type W-Zn deposits, hydrothermal vein-type Pb-Zn deposits, and hydrothermal vein-type independent Ag deposits (Jiang et al., 2015; Lei, 2012; Li et al., 2016). According to Yuan et al. (1990), the hidden granite pluton and ore deposits exhibit a special spatial relationship, i.e., the ore deposits are mainly hosted in the strata overlying the hidden granite body. As noticed in Fig. 2, these deposits have formed a typical mineralization zoning pattern around the bulge of the hidden pluton: from the pluton outward, mineralization type changes successively from W mineralization (e.g., at the Luowei deposit) through Pb-Zn mineralization (e.g., at the Lujing deposit) to Ag mineralization (e.g., at the Fenghuangshan deposit). Such a W-Pb-Zn-Ag polymetallic mineralization zoning pattern around the granitic plutons have been widely reported in China and the world (e.g., Chen et al., 2013; Pirajno, 2013; Mi et al., 2014; Cao et al., 2015; Zhao et al., 2018). The genesis of mineralization zoning pattern is usually associated with granitic magma-controlled hydrothermal mineralization systems (Park, 1955; Pirajno, 1992). For instance, the adjacent Damingshan region shows successively mineralized characteristics of W mineralization, Cu mineralization, Pb, Zn and Au mineralization around the Kunlunshan granite pluton (Li et al., 2008a; Yang et al., 2011). The Bozhushan W-Sn-Fe deposits were formed at the contact zone between the granite pluton and country rocks. Pb-Zn deposits were produced in the proximal area, and Sb deposits were generated in a more distal position of the pluton, in the southeastern Yunnan Province (Chen et al., 2015). The porphyry-skarn type W-Mo deposit, skarn type Zn-polymetallic deposit and hydrothermal type Pb-Zn-Ag deposit are successively distributed from the granite porphyry center outward to the Luanchuan area of Henan Province (Cao et al., 2015). W-(Mo)-Pb-Zn-Ag mineralization related to I-type granite porphyry is associated with a spatial zoning of Mo deposits in the center and Ag-Pb-Zn deposits in the distal distance in the Qinling-Dabie region (Li et al., 2008b).

It is widely accepted that granite composition varies with distinct diversities in metallogenetic specialization (Zhou and Huang, 1997; Wang et al., 2014). Our geochemical analyses show that all fresh granite samples exhibit peraluminous and high-K calc-alkaline affinities with ASI [molar $\text{Al}_2\text{O}_3/(\text{CaO} + \text{K}_2\text{O} + \text{Na}_2\text{O})$] = 1.46 – 1.61, enrichment in Rb, Th, U, and K, and depletion in Nb, Ta, P, and Ti. The results clearly show Xidamingshan hidden granite is S-type granite (Figs. 7, 8, 9). In South China, S-type granites and granitoids are nearly always associated with W-polymetallic mineralization (Blevin and Chappell, 1995; Zhou and Huang, 1997; Wang and Wang, 2001; Robb, 2005; Teixeira et al., 2012; Maulana et al., 2013; Wang et al., 2014; Huang et al., 2017a; Zhu et al., 2018). Other mineralized S-type granites include the Qianlishan granites (Mao and Li, 1995; Mao et al., 1995a; Shen et al., 1995; Cheng et al., 2013; Tong et al., 2013; Wan et al., 2013), Yaogangxian granites (Li, 2011; Dong et al., 2014) and Sheshan granitoids (Chen et al., 2012). In general, the granites related to W-polymetallic mineralization are of peraluminous and differentiated (Hua et al., 2010), with typical geochemical signatures showing low $\text{CaO}/(\text{Na}_2\text{O} + \text{K}_2\text{O})$ ratios, LREE/HREE ratios and δEu values, high Rb/Sr ratios, and strong Ba, Sr, P, and Ti depletions. The Xidamingshan hidden granite shares these geochemical signatures. Particularly, the Xidamingshan hidden granite

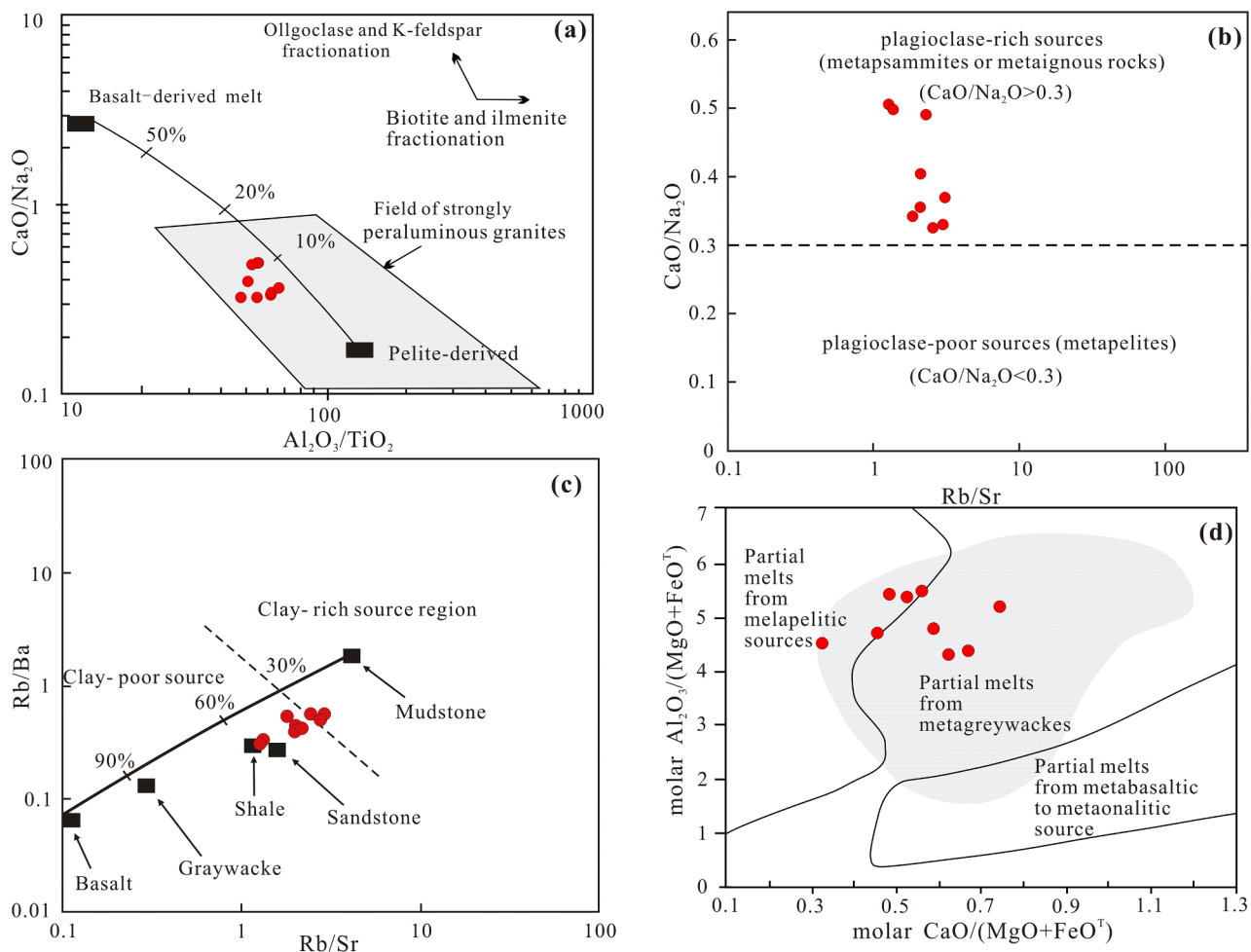


Fig. 16. Diagrams showing geochemical variations of the Xidamingshan hidden granite. (a) $\text{Al}_2\text{O}_3/\text{TiO}_2$ vs. $\text{CaO}/\text{Na}_2\text{O}$ diagram; (b) Rb/Sr vs. $\text{CaO}/\text{Na}_2\text{O}$ diagram; (c) Rb/Sr vs. Rb/Ba ; (d) molar $\text{CaO}/(\text{MgO} + \text{FeO}^\text{T})$ vs. molar $\text{Al}_2\text{O}_3/(\text{MgO} + \text{FeO}^\text{T})$.

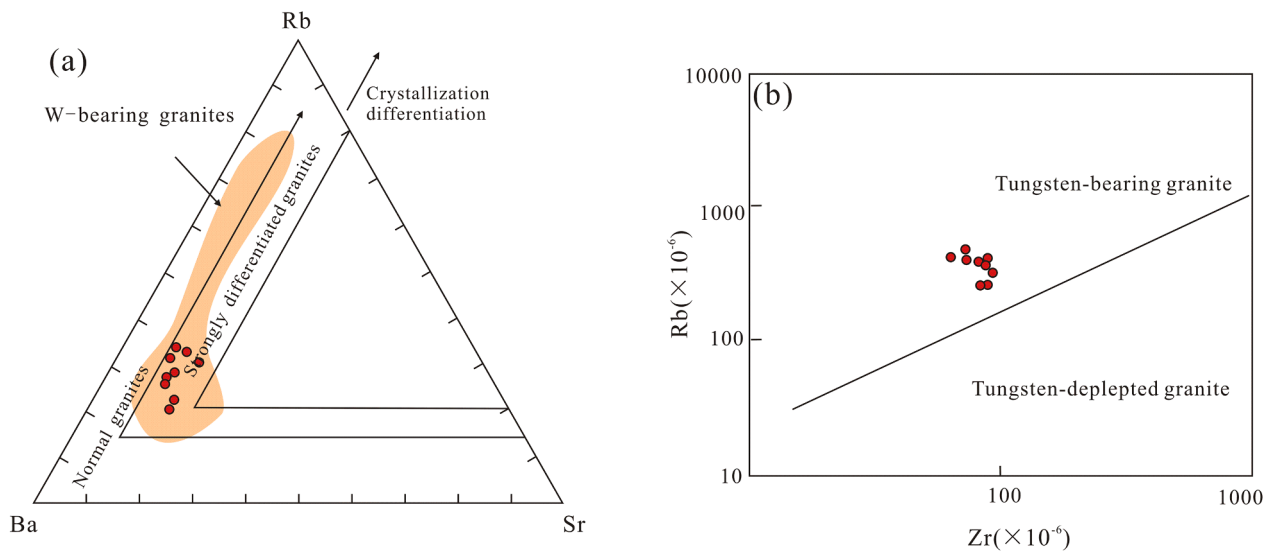


Fig. 17. Zr vs. Rb discrimination diagram.

is similar to a differentiated granite in composition (Fig. 17a). Moreover, the Xidamingshan hidden granite samples mostly plotted within the W-mineralization granite field within tungsten-bearing granite plots which are used to evaluate the W-polymetallic prospectivity of granitic stocks

(Figs. 17 a, b, and 18; Meinert, 1995; Srivastava and Sinha, 1997).

The Xidamingshan hidden granite is, therefore, interpreted to be genetically responsible for the occurrence of the W-Pb-Zn-Ag polymetallic deposits hosted in its overlying Cambrian strata (Fig. 19), as

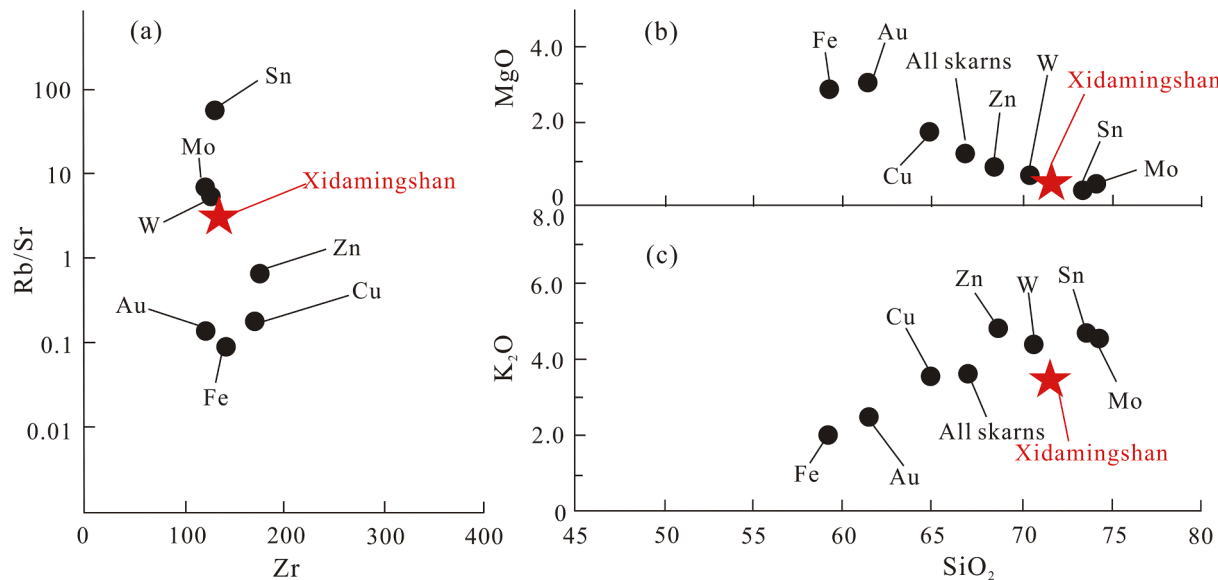


Fig. 18. Rb/Sr vs. Zr correlation diagram (a) and Harker variation diagrams of MgO vs. SiO₂ (b) and K₂O vs. SiO₂ (c) (after Meinert et al. 1995).

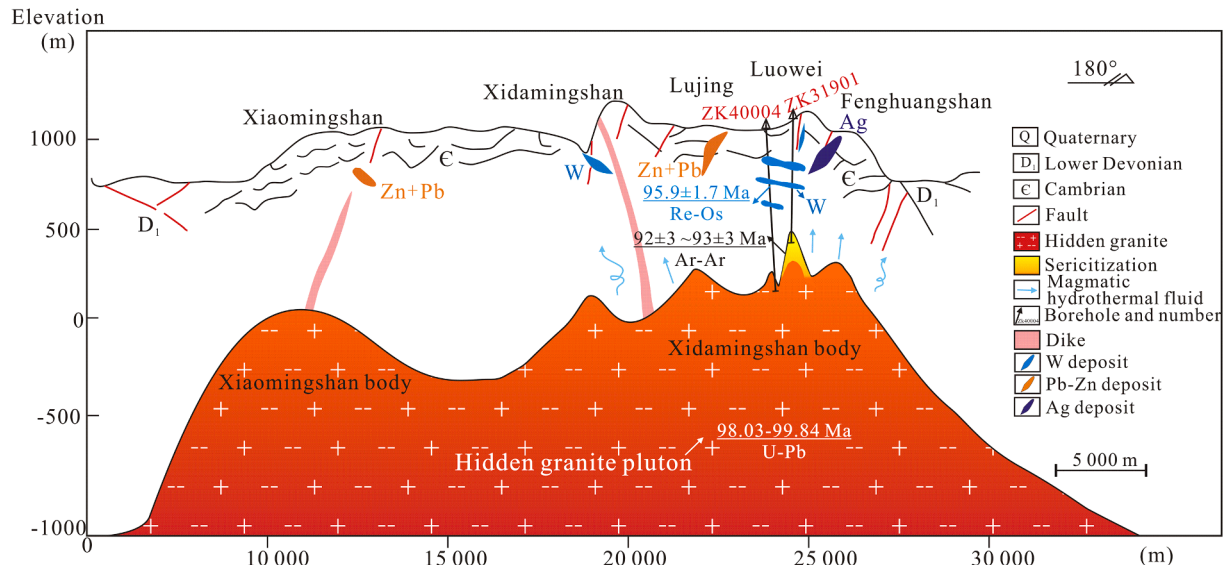


Fig. 19. A conceptual model showing spatial and genetic associations between the Xidamingshan hidden granite pluton and the regional W-Pb-Zn-Ag mineralization.

evidenced by the W-polymetallic specialization of the studied granitic pluton, the presence of intensive post-magmatic hydrothermal alteration indicated by Ar-Ar dating, as well as the mineralization zoning around the bulge of the hidden granite pluton.

Molybdenite from the Luowei deposit returned Re-Os isochron age of 95.9 ± 1.7 Ma. This age is consistent with the well-constrained LA-ICP-MS zircon U-Pb ages acquired on the hidden granite pluton. Such overlap indicates that close temporal and probable genetic relationship between the mineralization and the hidden granite pluton.

To a broad scale, the 99 – 92 Ma age of the Xidamingshan hidden granite pluton and its subsequent hydrothermal mineralization are coincident with the widespread Late Cretaceous (135 – 80 Ma) magmatism-mineralization event in South China (Hua et al., 2005; Mao et al., 2013). The emergence of Late Cretaceous granitic magmatism and related W-Sn-Pb-Zn-Ag-Au polymetallic mineralization in South China are considered to link to the extensional tectonics caused by subduction of the Pacific plate (e.g., Mao et al., 2013; Lecumberri-Sánchez et al., 2014; Chen et al., 2015; Cai et al., 2017).

It is worthy to note that the W-polymetallic deposits in the Xidamingshan region share many similarities of mineralization to other W-polymetallic deposits formed during the Cretaceous mineralization peak in South China. However, a complete hydrothermal mineralization system from proximal W deposits through Pb-Zn deposit to distal independent Ag deposits is relatively rarely reported in South China. Our result show that an intact W-Pb-Zn-Ag hydrothermal system may be connected to a deep sited pluton (buried deeper than 500 m). A large number of W-Pb-Zn-Ag deposits situated in the western segment of South China block (such as the Wutong deposit, [Lecumberri-Sanchez et al., 2014](#)) likely represent the shallow expression of the hidden granite-related mineralization systems, and more W or Sn deposits likely exist at deeper levels below surface.

7. Conclusions

The findings of this study provide a multi-dimensional picture of the deeply hidden granite pluton in the Xidamingshan W-Zn-Pb-Ag

mineralization district:

- (1) New LA-ICP-MS zircon U-Pb ages (98.0 ± 1.0 Ma and 99.8 ± 0.9 Ma) and muscovite ^{40}Ar - ^{39}Ar ages (93 ± 3 Ma and 92 ± 3 Ma) show that the Xidamingshan hidden biotite granite pluton was emplaced at late Cretaceous time. The emplacement was subsequently followed by hydrothermal alterations and mineralization. The molybdenite Re-Os isochronal age of 95.9 ± 1.7 Ma (MSWD = 2.2), indicates a close temporal relationship between the mineralization and the hidden granite pluton.
- (2) Lithogeochemical and Hf isotopic compositions demonstrate that the Xidamingshan hidden granite exhibits typical S-type granite nature, and that the granitic magmas were derived from Proterozoic crustal material of argillaceous-depleted sedimentary rocks. The nature and origin of this type of granites are known for W-polymetallic mineralization affinity when compared with other ore-forming granites in South China.
- (3) Significant polymetallic mineralization is present within the thick Cambrian strata that overly the hidden granite pluton, and distribution of the known deposits demonstrates a typical zoning pattern from skarn-type W deposits through vein-type Pb-Zn deposits to vein-type Ag deposits. Combined with all the evidences from metallogenic specialization of the granitic source rocks, geochronological coupling of the magmatism and hydrothermal activity, it is inferred that there exists a hydrothermal mineralization system driven by the emplacement of the Late Cretaceous S-type hidden granite pluton in the region.
- (4) The revelation of the close spatial and metallogenic associations between the hidden granite pluton and the W-Pb-Zn-Ag mineralization, especially the vertical variation from Zn-Pb-Ag mineralization at shallower levels to W mineralization at deeper levels, in this study, helps guide future deep drilling and exploration in areas with deeply hidden granitic plutons in South China and other similar regions worldwide.

Declaration of Competing Interest

The authors declare that they have no known competing financial interests or personal relationships that could have appeared to influence the work reported in this paper.

Acknowledgements

This research was financially supported by the Training Program of the Major Research Plan of the National Natural Science Foundation of China (91962107), Guangxi Natural Science Foundation (2018GXNSFAA050016; 2019JJA150083), Research Project of the Guangxi Prospecting Breakthrough Strategic Action (No. [2020]1639), the open research grant of Guangxi Key Laboratory of Hidden Metallic Ore Deposits Exploration (No. 20-065-17-K01), and the Collaborative Innovation Center for Exploration of Hidden Nonferrous Metal Deposits and Development of New Materials of Guangxi. We thank the editor and two anonymous reviewers for their constructive reviews and suggestions that help improve the original manuscript.

References

- Andersen, T., 2002. Correction of common lead in U-Pb analyses that do not report ^{204}Pb . *Chem. Geol.* 192, 59–79.
- Bi, S.J., Yang, Z., Li, W., Li, T., Liang, P., Tang, K.F., 2015. Discovery of late Cretaceous Baoshan porphyry copper deposit in Dayaoshan, Qinhang metallogenic belt: constraints from Zircon U-Pb age and Hf isotope. *J. China Univ. Geosci. (Earth Sci. Ed.)* 40, 1458–1479 (in Chinese with English abstract).
- Blevin, P.L., Chappell, B.W., 1995. Chemistry, origin, and evolution of mineralized granites in the Lachlan fold belt, Australia; the metallogeny of I- and S-type granites. *Econ. Geol.* 90, 1640–1649.
- Blichert-Toft, J., Albarède, F., 1997. The Lu-Hf isotope geochemistry of chondrites and the evolution of the mantle-crust system. *Earth Planet. Sci. Lett.* 148 (1–2), 243–258.
- Boynton, W.V., 1984. Cosmochemistry of the rare earth elements: meteorites studies. In: Henderson, P. (Ed.), *Rare Earth Element Geochemistry*. Elsevier, Amsterdam, pp. 63–114.
- Cai, M.H., He, L.Q., Li, G.Q., Wu, D.C., Huang, H.M., 2006. SHRIMP Zircon U-Pb dating of the intrusive rocks in the Dachang tin-polymetallic ore field, Guangxi and their geological significance. *Geol. Rev.* 52, 409–414 (in Chinese with English abstract).
- Cai, M.H., Feng, Z.H., Shao, T.B., Hu, R.G., Zhou, Y., Xu, J.F., 2017. New precise zircon U-Pb and muscovite ^{40}Ar - ^{39}Ar geochronology of the Late Cretaceous W-Sn mineralization in the Shanhу orefield, South China. *Ore Geol. Rev.* 84, 338–346.
- Cao, H.W., Zhang, S.T., Santosh, M., Zheng, L., Tang, L., Li, D., Zhang, X.H., Zhang, Y.H., 2015. The Luanchuan Mo-W-Pb-Zn-Ag magmatic-hydrothermal system in the east Qinling metallogenic belt, China: constrains on metallogenesis from C-H-O-S-Pb isotope compositions and Rb-Sr isochron ages. *J. Asian Earth Sci.* 111, 751–780.
- Chai, M.C., Fu, W., Feng, Z.H., Xu, W.Z., Le, X.W., Li, S.S., Lu, J.H., Liu, W.W., Pang, Y.Q., 2015. Characteristics of ore-forming fluids of Nongtun Pb-Zn deposit in Xidamings Mountain of Guangxi and their implications for ore genesis. *Miner. Deposits* 5, 948–964 (in Chinese with English abstract).
- Charvet, J., Faure, M., Fabbri, O., Cluzel, D., Lapierre, H., 1990. Accretion and collision during East-Asian margin building: a new insight on the Peri-Pacific orogenies. In: Wiley, T.J., Howell, D.G., Wong, F.L. (Eds.), *Terrane Analysis of China and the Pacific Rim: Circum-Pacific Council for Energy and Mineral Resources, Earth Science Series* 13, pp. 161–190.
- Chappell, B.W., White, A.J.R., 1974. Two contrasting granite types. *Pacific Geology* 8, 173–174.
- Chappell, B.W., White, A.J.R., 1992. I- and S-type granites in the Lachlan Fold Belt. *Geol. Soc. Am. Spec. Pap.* 272, 1–26.
- Chappell, B.W., 1999. Aluminium saturation in I- and S-type granites and the characterization of fractionated haplogranites. *Lithos* 46, 535–551.
- Chen, J.F., Jahn, B.M., 1998. Crustal evolution of southeastern China: Nd and Sr isotopic evidence. *Tectonophysics* 284, 101–133.
- Chen, F.W., Li, H.Q., Mei, Y.P., 2008. Zircon SHRIMP U-Pb chronology of diagenetic mineralization of the Longtoushan porphyry gold orefield, Gui County, Guangxi. *Acta Geol. Sin.* 82, 921–926 (in Chinese with English abstract).
- Chen, X.C., Hu, R.Z., Bi, X.W., Zhong, H., Lan, J.B., Zhao, C.H., Zhu, J.J., 2015a. Zircon U-Pb ages and Hf-O isotopes, and whole-rock Sr-Nd isotopes of the Bozhushan granite, Yunnan province, SW China: constraints on petrogenesis and tectonic setting. *J. Asian Earth Sci.* 99, 57–71.
- Chen, M.H., Zhang, W., Yang, Z.X., Lu, G., Hou, K.J., Liu, J.H., 2009. Zircon SHRIMP U-Pb age and Hf isotopic composition of Baiceng ultrabasic dykes in Zhenfeng county, southwestern Guizhou Province. *Miner. Depos.* 28, 240–250 (in Chinese with English abstract).
- Chen, M.H., Mo, C.S., Huang, Z.Z., Li, B., Huang, R.W., 2011. Zircon LA-ICP-MS U-Pb ages of granitoid rocks and molybdenite Re-Os age of Shedong W-Mo deposit in Cangwu County of Guangxi and its geological significance. *Miner. Deposits* 30, 963–978 (in Chinese with English abstract).
- Chen, M.H., Huang, Z.Z., Li, B., Huang, H.W., 2012. Geochemistry of granitoid rocks of Shedong W-Mo deposit district in Cangwu County, Guangxi and its relation to mineralization. *Acta Petrologica Sinica* 28 (1), 199–212.
- Chen, J., Wang, R.C., Zhu, J.C., Lu, J.J., 2013. Multiple-aged granitoids and related tungsten-tin mineralization in the Nanling range, South China. *Science China: Earth Sciences* 56, 2045–2055.
- Chen, M.H., Li, Z.Y., Li, Q., 2015b. A preliminary study of multi-stage granitoids and related metallogenic series in Dayaoshan area of Guangxi, China. *Earth Sci. Front.* 22, 41–53 (in Chinese with English abstract).
- Cheng, Y.B., Mao, J.W., 2010. Age and geochemistry of granites in Gejju area, Yunnan province, SW China: constraints on their petrogenesis and corresponding tectonic setting. *Lithos* 120, 258–276.
- Cheng, Y.S., Tan, R.F., Wan, Y., 2013. Petrological and geochemical characteristics of the Qianlishan granite in south Hunan Province. *Acta Miner. Sin. S2*, 579–580 (in Chinese with English abstract).
- Çimen, O., Göncüoğlu, M.C., Simonetti, A., Sayit, K., 2018. New zircon U-Pb LA-ICP-MS ages and Hf isotope data from the Central Pontides (Turkey): Geological and geodynamic constraints. *Journal of Geodynamics* 116, 23–26.
- Clemens, J.D., 2003. S-type granitic magmas-petrogenetic issues, models and evidence. *Earth Sci. Rev.* 61, 1–18.
- Collins, W.J., Beams, S.D., White, A.J.R., 1982. Nature and origin of A-type granites with particular reference to southeastern Australia. *Contributions to Mineralogy and Petrology* 80, 189–200.
- Cui, B., Zhai, Y.S., Meng, Y.F., Huang, F.F., Shu, B., Liu, G.H., 2000. Transformation of Mesozoic tectonic domain and its relation to mineralization in southeastern China: an evidence of southwestern Fujian Province. *J. China Univ. Geosci. (Earth Sci. Ed.)* 25, 352–396 (in Chinese with English abstract).
- Dalrymple, B.G., Lanphere, M.A., 1971. ^{40}Ar - ^{39}Ar technique of K-Ar dating: a comparison with the conventional technique. *Earth Planet. Sci. Lett.* 12, 300–308.
- Dodson, M.H., McClelland-Brown, E., 1985. Isotopic and palaeomagnetic evidence for rates of cooling, uplift and erosion. *Geol. Society of London* 10, 315–325.
- Dong, S.H., Bi, X.W., Hu, R.Z., Chen, Y.W., 2014. Petrogenesis of the Yaogangxian granites and implications for W mineralization, Hunan Province. *Acta Petrol. Sin.* 30, 2749–2765 (in Chinese with English abstract).
- Du, A.D., Wu, S.Q., Sun, D.Z., Wang, S.X., Qu, W.J., Markey, R., Stain, H., Morgan, J., Malinovskiy, D., 2004. Preparation and Certification of Re-Os Dating Reference Materials: Molybdenites HLP and JDC. *Geostand. Geoanal. Res.* 28, 41–52.
- Duan, R.C., Ling, W.L., Li, Q., Chen, Z.W., Yang, H.M., Liu, L.F., 2011. Correlations of the late Yanshanian tectonomagmatic events with metallogenesis in South China: geochemical constraints from the Longtoushan gold ore deposit of the Dayaoshan area, Guangxi Province. *Acta Geol. Sinica* 85, 1644–1658.

- Feng, J.R., Mao, J.W., Pei, R.F., et al., 2011. A tentative discussion on Indosinian ore-forming events in Laojunshan area of southeastern Yunnan: A case study of Xinzhai tin deposit and Nanyangtian tungsten deposit. *Min. Depos.* 30, 57–73 (in Chinese with English abstract).
- Geng, H.Y., Xu, X.S., O'Reilly, S.Y., Zhao, M., Sun, T., 2006. Cretaceous volcanic-intrusive magmatic activity and its geological significance in western Guangdong. *Sci. China Series D: Earth Sci.* 70, 26–43.
- Goldfarb, R.J., Hart, C.J.R., Mao, J., Hofstra, A.H., 2004. Gold in China – the present understanding of emerging world-class resources. In: McPhie, J., McGoldrick, P. (Eds.), *Dynamic Earth: Past, Present and Future*, 17th Australian Geological Convention, 8–13 February, 2004. Geological Society of Australia Abstract, vol. 73, p. 82.
- Griffin, W.L., Pearson, N.J., Belousova, E., Jackson, S.E., Van Achterbergh, E., O'Reilly, S.R., 2000. The Hf isotope composition of cratonic mantle: LAM-MC-ICPMS analysis of zircon megacrysts in kimberlites. *Geochim. Cosmochim. Acta* 64, 133–147.
- Griffin, W.L., Wang, X., Jackson, S.E., Pearson, N.J., O'Reilly, S.Y., Xu, X., Zhou, X., 2002. Zircon chemistry and magma mixing, SE China: in-situ analysis of Hf isotopes, Tonglu and Pingtan igneous complexes. *Lithos* 61, 237–269.
- Guangxi BGMR (Bureau of Geology and Mineral Resources of Guangxi Province), 1985. Regional geology of Guangxi province. Beijing Geological Publishing House, 256p (in Chinese with English abstract).
- Guangxi GSI (Geophysical Survey Institute of Guangxi Province), 1984. Preliminary study on geological significance of gravity field in Guangxi. (in Chinese with English abstract).
- Guo, C.L., Chen, Y.C., Zeng, Z.L., Lou, F.S., 2012. Petrogenesis of the Xihuashan granites in southeastern China: Constraints from geochemistry and in-situ analyses of zircon U-Pb-Hf-O isotopes. *Lithos* 148, 209–227.
- Hine, B.Y., Williams, I.S., Chappell, B.W., White, A.J.R., 1978. Contrasts between I-and S-type granitoids of the Kosciusko batholith. *J. Geol. Soc. Australia* 25, 219–234.
- Hu, R.Z., Bi, X.W., Jiang, G.H., Chen, Y.W., Peng, J.T., Qi, Y.Q., Wu, L.Y., Wei, W.F., 2012b. Mantle-derived noble gases in ore-forming fluids of the granite-related Yaogangxian tungsten deposit, southeastern China. *Miner. Depos.* 47, 623–632.
- Hu, R.Z., Wei, W.F., Bi, X.W., Peng, J.T., Qi, Y.Q., Wu, L.Y., Chen, Y.W., 2012c. Molybdenite Re-Os and muscovite $^{40}\text{Ar}/^{39}\text{Ar}$ dating of the Xihuashan tungsten deposit, central Nanling district, South China. *Lithos* 150, 111–118.
- Hu, S.Q., Zhu, Q., Zhang, X.J., Yi, S.H., Peng, S.B., Zhou, G.F., Wu, L.B., Chen, H.H., 2013. Geochronology, geochemistry and zircon Hf isotope of granite porphyry in Yuanzhudong Cu-Mo deposit, Guangdong Province. *Miner. Deposits* 32, 1139–1158 (in Chinese with English abstract).
- Hu, R.Z., Chen, W.T., Xu, D.R., Zhou, M.F., 2017. Reviews and new metallogenetic models of mineral deposits in South China: An introduction. *J. Asian Earth Sci.* 137, 1–8.
- Hua, R.M., Chen, P.R., Zhang, W.L., Lu, J.J., 2005. Three major metallogenetic events in Mesozoic in South China. *Miner. Depos.* 24, 99–107 (in Chinese with English abstract).
- Hua, R.M., Li, G.L., Zhang, W.L., Hu, D.Q., Chen, P.R., Chen, W.F., Wang, X.D., 2010. A tentative discussion on differences between large-scale tungsten and tin mineralization in South China. *Miner. Deposits* 29, 9–23 (in Chinese with English abstract).
- Huang, Q.X., 1994. Concealed granite bodies in Guangxi and their ore-prospecting significance. *Geophysical and Geochemical Exploration* 18, 61–70 (in Chinese English abstract).
- Huang, J.Z., 2008. Geological characteristics and prospecting potential of Mutuoshan Ag deposit in Longan County, Guangxi. *Land and resources of southern China* 3, 22–24 (in Chinese English abstract).
- Huang, Z.H., Li, Z.Y., Shi, Y.C., Huang, Z.G., Huang, X.Y., 2015. The instruction function and analysis of mineralization potential for deep prospecting in Luowei ore mine from results of geophysical prospecting. *Gold Science and Technology*, 23, 53–60 (in Chinese with English abstract).
- Huang, X.D., Lu, J.J., Sizaret, S., Wang, R.C., Ma, D.S., Zhang, R.Q., Zhao, X., Wu, J.W., 2017a. Petrogenetic differences between the Middle-Late Jurassic Cu-Pb-Zn-bearing and W-bearing granites in the Nanling Range, South China: A case study of the Tongshanling and Weijia deposits in southern Hunan Province. *Sci. China Series D: Earth Sci.* 60, 1220–1236.
- Huang, W.T., Wu, J., Zhang, J., Liang, H.Y., Qiu, X.L., 2017b. Geochemistry and Hf-Nd isotope characteristics and forming processes of the Yuntoujue granites associated with W-Mo deposit, Guangxi. *Ore Geol. Rev.* 81, 953–964.
- Jiang, S.Y., Zhao, K.D., Jiang, Y.H., Ling, H.F., Ni, P., 2006. New type of tin mineralization related to granite in South China: evidence from mineral chemistry, element and isotope geochemistry. *Acta Petrol. Sin.* 22 (10), 2509–2516 (in Chinese with English abstract).
- Jiang, S.Y., Peng, N.J., Huang, L.C., Xu, Y.M., Zhan, G.L., Dan, X.H., 2015. Geological characteristic and ore genesis of the giant tungsten deposits from the Dahutang ore-concentrated district in northern Jiangxi province. *Acta Petrol. Sin.* 31 (3), 639–655 (in Chinese with English abstract).
- Jin, X.D., Zhang, D.H., Wan, T.F., 2010. Upper part and deeper area ore-prospecting for hidden rock mass. *Geol. Bull. China* 2, 392–400.
- Kinny, P.D., Maas, R., 2003. Lu-Hf and Sm-Nd isotope systems in zircon. *Rev. Mineral. Geochem.* 53, 327–341.
- King, P.L., White, A.J.R., Chappell, B.W., Allen, C.M., 1997. Characterization and origin of aluminous A-type granite from the Lachlan fold belt, Southeastern Australia. *J. Petrol.* 38, 371–391.
- Knudsen, T.L., Griffin, W., Hartz, E., Andresen, A., Jackson, S., 2001. In-situ hafnium and lead isotope analyses of detrital zircons from the Devonian sedimentary basin of NE Greenland: A record of repeated crustal reworking. *Contributions to Mineralogy and Petrology* 141, 83–94.
- Lei, Y.P., 2012. Mineral prediction of the Xidamingshan silver polymetallic ore district, Guangxi. PhD dissertation, China University of Geosciences (Beijing) (in Chinese with English abstract).
- Lecumberri-Sanchez, P., Romer, R.L., Lüders, V., Bodnar, R.J., 2014. Genetic relationship between silver-lead-zinc mineralization in the Wutong deposit, Guangxi Province and Mesozoic granitic magmatism in the Nanling belt, southeast China. *Mineral. Deposita* 49, 353–369.
- Lees, B., Behling, S., Misantoni, D., Lueders, V., Romer, R.L., Sanchez, P.L., Cory, P., 2011. The Wutong mine; Guangxi Zhuang Autonomous region, China. *Mineral Rec.* 42, 521–544.
- Li, Z.X., Li, X.H., Zhou, H., Kinny, P.D., 2002. Grenvillian continental collision in south China: new SHRIMP U-Pb zircon results and implications for the configuration of Rodinia. *Geology* 30, 163–166.
- Li, X.H., Li, Z.X., Li, W.X., Wang, Y., 2006. Initiation of the Indosinian orogeny in South China: Evidence for a Permian magmatic arc on Hainan Island. *The Journal of Geology* 114, 341–353.
- Li, X.H., Li, W.X., Li, Z.X., 2007a. On the genetic classification and tectonic implications of the Early Yanshanian granitoids in the Nanling Range, South China. *Chin. Sci. Bull.* 52, 1873–1885.
- Li, X.H., Li, Z.X., Li, W.X., Liu, Y., Yuan, C., Wei, G.J., Qi, C.S., 2007b. U-Pb zircon, geochemical and Sr-Nd-Hf isotopic constraints on age and origin of Jurassic I- and A-type granites from central Guangdong, SE China: a major igneous event in response to fountaining of a subducted flat-slab. *Lithos* 96, 186–204.
- Li, S.R., Wang, D.H., Liang, T., Qu, W.J., Ying, L.J., 2008a. Metallogenetic epochs of the Damingshan tungsten deposit in Guangxi and its prospecting potential. *Acta Geol. Sin.* 7, 873–879 (in Chinese with English abstract).
- Li, H.M., Chen, Y.C., Ye, H.S., Wang, D.H., Guo, B.J., Li, Y.F., 2008b. Mo, (W), Au, Ag, Pb, Zn minerogenetic series related to Mesozoic magmatic activities in the east Qinling-Dabie Mountains. *Acta Geol. Sin.* 82 (11), 1468–1477 (in Chinese with English abstract).
- Li, X.H., Long, W.G., Li, Q.L., Liu, Y., Zheng, Y.F., Yang, Y.H., Chamberlain, K.R., Wan, D.F., Guo, C.H., Wang, X.C., Tao, H., 2010. Penglai zircon megacrysts: A potential new working reference material for microbeam determination of Hf-O isotopes and U-Pb age. *Geostandards and Geoanalytical Research* 34, 117–134.
- Li, S.T., 2011. Characteristics and genesis of the Yaogangxian tungsten polymetallic deposit in Hunan. China University of Geosciences (Beijing) (in Chinese with English abstract).
- Li, S., Feng, Z.H., Fu, W., Jia, Z.Q., Long, M.Z., Liu, W.W., Peng, Z.Y., Li, Y.J., 2016. A practice of the Comprehensive Geological-Geophysical-Geochronological Methods on searching for Concealed Rock Mass—A Case Study of concealed rock mass in Xidamingshan, Guangxi. *Geology and Exploration* 52, 524–536 (in Chinese with English abstract).
- Li, S., Feng, Z.H., Shan, Y.P., Fu, W., Le, X.W., Liu, W.W., Xu, W.Z., 2017. Fracture structural analysis of Nongtun Pb-Zn deposit in Xidamingshan, Guangxi. *Miner. Deposits* 16, 275–290 (in Chinese with English abstract).
- Liang, S.Y., Yang, X., 2004. Geochemical characteristics and prospecting potential of Ag-Pb-Zn in the Xidamingshan upwelling area. *Land. Resour. South. China* 4, 22–24 (in Chinese with English abstract).
- Liu, S., Su, W.C., Hu, R.Z., Feng, C.J., Gao, S., Coulan, I.M., Wang, T., Feng, G.Y., Tao, Y., Xia, Y., 2010. Geochronological and geochemical constraints on the petrogenesis of alkaline ultramafic dykes from southwest Guizhou Province, SW China. *Lithos* 114, 253–264.
- Liu, P., Mao, J.W., Cheng, Y.B., Yao, W., Wang, X.Y., Hao, D., 2017. An early Cretaceous W-Sn deposit and its implications in southeast coastal metallogenetic belt: Constraints from W-Pb, Re-Os, Ar-Ar geochronology at the Feie'shan W-Sn deposit, SE China. *Ore Geol. Rev.* 81, 112–122.
- Lu, J.H., 2015. Geological characteristics, metallogenetic regularity and metallogenetic model of Xidamingshan Ag-Pb-Zn-Au-W-Bi deposit. *Miner. Resour. Geol.* 5, 560–567 (in Chinese with English abstract).
- Ludwig, K.R., 2003. ISOPLOT 3.0: a geochronological toolkit for Microsoft Excel. Berkeley Geochronology Center. Special publication no. 4.
- Luo, J.H., Che, Z.C., Guo, A.L., Chen, S.Y., Pei, X.Z., 2009. Late Cretaceous lithospheric extension in the Nandan-Hechi tectonic zone of northern Guangxi Province and its influence on hydrocarbon accumulation conditions. *Oil. Gas Geol.* 30, 619–625 (in Chinese with English abstract).
- Mai, G.T., 1990. On evolution distribution and emplacement of granites of granite based on the regional gravitational-magnetic field in Guangxi. *Geology of Guangxi* 1, 15–23 (in Chinese with English abstract).
- Maniar, P.D., Piccoli, P.M., 1989. Tectonic discrimination of granitoids. *Geological Society of America* 101, 635–643.
- Mao, J.W., Li, H.Y., 1995. Evolution of the Qianlishan granite stock and its relation to the Shizhuyuan polymetallic tungsten deposit. *Int. Geol. Rev.* 37, 63–80.
- Mao, J.W., Li, H.Y., Pei, R.F., 1995a. Geology and geochemistry of the Qianlishan granite stock and its relationship to polymetallic tungsten mineralization. *Miner. Deposits* 14, 12–25 (in Chinese with English abstract).
- Mao, J.W., Guy, G., Rimbault, L., Shimazaki, H., 1996a. Manganese skarn in the Shizhuyuan polymetallic deposit, Hunan, China. *Resour. Geol.* 46, 1–11.
- Mao, J.W., Li, H.Y., 1996b. Geology and metallogeny of the Shizhuyuan skarn-greisen deposit, Hunan Province, China. *Int. Geol. Rev.* 38, 1020–1039.
- Mao, J.W., Li, X.F., Lehmann, B., Chen, W., Lan, X.M., Wei, S.L., 2004. $^{40}\text{Ar}/^{39}\text{Ar}$ dating of tin ores and related granite in Furong tin orefield, Hunan province, and its geodynamic significance. *Miner. Deposits* 23, 164–175 (in Chinese with English abstract).
- Mao, J.W., Zhang, J.D., Pirajno, F., Lshiyama, D., Su, H.M., Guo, C.L., Chen, Y.C., 2011. Porphyry Cu-Au-Mo-epithermal Ag-Pb-Zn-distal hydrothermal Au deposits in the

- Dexing area, Jiangxi province, East China – A linked ore system. *Ore Geol. Rev.* 43, 203–216.
- Mao, J.W., Cheng, Y.B., Chen, M.H., Pirajno, F., 2013. Major types and time-space distribution of Mesozoic ore deposits in South China and their geodynamic settings. *Miner. Deposita* 48, 267–294.
- Maruyama, S., Isozaki, Y., Kimura, G., Terabayashi, M., 1997. Paleogeographic maps of the Japanese Islands: plate tectonic synthesis from 750 Ma to the present. *Island Arc* 6, 121–142.
- Maulana, A., Watanabe, K., Imai, A., Yonezu, K., 2013. Origin of magnetite- and ilmenite-series granitic rocks in Sulawesi, Indonesia: magma genesis and regional metallogenic constraint. *Procedia Earth. Planet. Sci.* 6, 50–57.
- Meinert, L.D., 1995. Compositional variation of igneous rocks associated with skarn deposits—chemical evidence for genetic connection between petrogenesis and mineralization. *Mineralogical Association of Canada Short Course Series* 23, 401–418.
- Mi, M., Chen, Y.J., Yang, Y.F., Wang, P., Li, F.L., Wan, S.Q., Xu, Y.L., 2014. Geochronology and geochemistry of the giant Qian'echong Mo deposit, Dabie Shan, eastern China: implications for ore genesis and tectonic setting. *Gondwana Res.* 27, 1217–1235.
- Middlemost, E.A.K., 1994. Naming materials in the magma/igneous rock system. *Earth-Sci Rev.* 37, 215–224.
- Park, C.F.J., 1955. The zonal theory of ore deposits. *Econ. Geol.* Fiftieth Anniversary, pp. 226–248.
- Patchett, P.J., Kouvo, O., Hedge, C.E., Tatsumoto, M., 1981. Evolution of continental crust and mantle heterogeneity: evidence from Hf isotopes. *Contrib. Mineral. Petro.* 78, 279–297.
- Peccerillo, A., Taylor, S.R., 1976. Geochemistry of Eocene calc-alkaline volcanic rocks from the Kastamonu area, Northern Turkey. *Contrib. Miner. Petro.* 58, 63–81.
- Peng, J.T., Zhou, M.F., Hu, R.Z., Shen, N.P., Yuan, S.D., Bi, X.W., Du, A.D., Qu, W.J., 2006. Precise molybdenite Re-Os and mica Ar-Ar dating of the Mesozoic Yaogangxian tungsten deposit, central Nanling district, South China. *Miner. Deposita* 41, 661–669.
- Peng, J.T., Hu, R.Z., Bi, X.W., Dai, T.M., Li, Z.L., Li, X.M., Shuang, Y., Yuan, S.D., Liu, S.R., 2007. $^{40}\text{Ar}/^{39}\text{Ar}$ isotopic dating of tin mineralization in Furong deposit of Hunan Province and its geological significance. *Miner. Deposits* 26, 237–248 (in Chinese with English abstract).
- Pirajno, F., 1992. Hydrothermal Mineral Deposits: Principles and Fundamental Concepts for the Exploration Geologist. Springer, Berlin, p. 709.
- Pirajno, F., 2013. The Geology and Tectonic Settings of China's Mineral Deposits. Springer Science + Business Media, Dordrecht.
- Pircher, W.S., 1983. Granite type and tectonic environment. In: Hsu, K. (Ed.), Mountain Building Processes. Academic Press, London, pp. 19–40.
- Renne, P.R., Mundil, R., Balco, G., Min, K., Ludwig, K.R., 2010. Joint determination of ^{40}K decay constants and $^{40}\text{Ar}^*/^{40}\text{K}$ for the Fish Canyon sanidine standard, and improved accuracy for $^{40}\text{Ar}/^{39}\text{Ar}$ geochronology. *Geochim. Cosmochim. Acta* 74, 5349–5367.
- Robb, L., 2005. Introduction to ore-forming processes. Blackwell Publishing Company, Oxford, UK, pp. 1–386.
- Rubatto, D., Gebauer, D., 2000. Use of cathodoluminescence for U-Pb zircon dating by ion microprobe: some examples from the Western Alps. *Cathodoluminescence in Geosciences*. Springer, Berlin, pp. 373–400.
- Selby, D., Creaser, R.A., 2001. Re-Os geochronology and systematics in molybdenite from the Endako porphyry molybdenum deposit, British Columbia, Canada. *Econ. Geol.* 96, 197–204.
- Selby, D., Creaser, R.A., Hart, C.J.R., Rombach, C.S., Thompson, J.F.H., Smith, M.T., Bakke, A.A., Goldfarb, R.J., 2002. Absolute timing of sulfide and gold mineralization: a comparison of Re-Os molybdenite and Ar-Ar mica methods from the Tintina Gold Belt, Alaska. *Geology* 30, 791–794.
- Shen, W.Z., Wang, D.Z., Xie, Y.L., Xie, C.S., 1995. Geochemical characteristics and material sources of the Qianlishan composite granite body, Hunan province. *Acta Petrol. Miner.* 14, 193–202 (in Chinese with English abstract).
- Shirey, S.B., Walker, R.J., 1995. Carius tube digestion for low-blank rhenium-osmium analysis. *Anal. Chem.* 67, 2136–2141.
- Shu, X.J., Wang, X.L., Sun, T., Xu, X.S., Dai, M.N., 2011. Trace elements, U-Pb ages and Hf isotopes of zircons from Mesozoic granites in the western Nanling Range, South China: implications for petrogenesis and W-Sn mineralization. *Lithos* 127, 468–482.
- Smoliar, M.I., Walker, R.J., Morgan, J.W., 1996. Re-Os ages of group IIA, IIIA, IVA, and IVB iron meteorites. *Science* 271, 1099–1102.
- Söderlund, U., Patchett, P.J., Vervoort, J.D., Elsachsen, C., 2004. The ^{176}Lu decay constant determined by Lu-Hf and U-Pb isotope systematics of Precambrian mafic intrusions. *Earth Planet. Sci. Lett.* 219, 311–324.
- Srivastava, P.K., Sinha, A.K., 1997. Geochemical characterization of tungsten-bearing granites from Rajasthan, India. *J. Geochem. Explor.* 60, 173–184.
- Steiger, R.J., Jäger, E., 1977. Subcommission on geochronology: Convention on the use of decay constants in geo- and cosmochronology. *Earth Planet. Sci. Lett.* 36, 359–362.
- Stein, H.J., Sundblad, K., Markey, R.J., Morgan, J.W., Motuzza, G., 1998. Re-Os ages for Archean molybdenite and pyrite, Kuittila-Kivisuo, Finland and Proterozoic molybdenite, Kabeliai, Lithuania: testing the chronometer in a metamorphic and metasomatic setting. *Miner. Deposita* 33 (4), 329–345.
- Stein, H.J., Markey, R.J., Morgan, J.W., Hannah, J.L., Scherstén, A., 2001. The remarkable Re-Os chronometer in molybdenite: how and why it works. *Terra Nova* 13, 479–486.
- Sun, S.S., and McDonough, W.F., 1989. Chemical and Isotopic Systematics of oceanic basalts: implications for Mantle Composition and Processes. In: Saunders, A.D., Norry, M.J. (Eds.), Magmatism in the Ocean Basins. *Geol. Soc. Lond. Spec. Publ.* Vol. 42, pp. 313–345.
- Sun, Y.L., Zhou, M.F., Sun, M., 2001. Routine Os analysis by isotope dilution-inductively coupled plasma mass spectrometry: OsO₄ in water solution gives high sensitivity. *J. Anal. At. Spectrom.* 16, 345–349.
- Sun, T., 2006. A new map showing the distribution of granites in South China and its explanatory notes. *Geol. Bullet. China* 25, 332–335 (in Chinese with English abstract).
- Sun, T., Xu, P., Li, J., He, K., Chu, Z.Y., Wang, C.Y., 2010. A practical method for determination of molybdenite Re-Os age by inductively coupled plasma-mass spectrometry combined with Carius tube-HNO₃ digestion. *Anal. Methods* 2, 575–581.
- Sylvester, P.J., 1998. Post-collision strongly peraluminous granites. *Lithos* 45, 29–44.
- Tan, J., Wei, J.H., Li, S.R., Wang, Z.M., Fu, L.B., Zhang, K.Q., 2008. Geochemical Characteristics and Tectonic Significance of Kunlunguan A-Type Granite, Guangxi. *Earth Science* 33, 743–754 (in Chinese with English abstract).
- Teixeira, R.J.S., Neiva, A.M.R., Gomes, M.E.P., Corfu, F., Cuesta, A., Croudace, I., 2012. The role of fractional crystallization in the genesis of early syn-D3, tin-mineralized Variscan two-mica granites from the Carrazeda de Ansiães area, northern Portugal. *Lithos* 153, 177–191.
- Tong, L.H., 2013. The petrogenesis and metallogenetic model of Qianlishan tin-tungsten bearing granite in Hunan. China University of Geosciences (Beijing) (in Chinese with English abstract), China.
- Wan, G.L., 2013. Hunan Qianlishan granite constraints on mineralization. China University of Geosciences (Beijing) (in Chinese with English abstract).
- Wang, D.H., Chen, Y.C., Chen, W., Sang, H.Q., Li, H.Q., Lu, Y.F., Chen, K.L., Lin, Z.M., 2004. Dating the Dachang giant tin-polymetallic deposit in Nandan, Guangxi. *Acta Geol. Sin.* 78, 132–139 (in Chinese with English abstract).
- Wang, D.Z., Liu, C.S., Shen, W.Z., Chen, F.R., 1993. The contrast between Tonglu I-type and Xiangshan S-type clastic-porphyritic lava. *Acta Petrol. Sin.* 9, 44–53 (in Chinese with English abstract).
- Wang, X.W., Wang, X.D., 2001. Geochemical signs of mineralized granite. *Geol. Miner. Resour. South China* 4, 36–44 (in Chinese with English abstract).
- Wang, D.Z., Zhou, J.C., 2005. New progress in studying the Large Igneous Provinces. *Geol. J. China Univ.* 11, 1–8 (in Chinese with English abstract).
- Wang, C.M., Zhang, D., Wu, G.G., Santos, M., Zhang, J., Xu, Y.G., Zhang, Y.Y., 2014a. Geological and isotopic evidence for magmatic-hydrothermal origin of the Ag-Pb-Zn deposits in the Lengshukeng District, east-central China. *Miner. Depos.* 49, 733–749.
- Wang, D.H., Chen, Z.Y., Huang, F., Wang, C.H., Zhao, Z., Chen, Z.H., Zhao, Z., Liu, X.X., 2014b. Discussion on metallogenetic specialization of the magmatic rocks and related issues in the Nanling region. *Geotectonica et Metallogenica* 38, 230–238 (in Chinese with English abstract).
- Wolf, M.B., London, D., 1994. Apatite dissolution into peraluminous haplo granitic melts: An experimental study of solubilities and mechanisms. *Geochim. Cosmochim. Acta* 58, 4127–4145.
- Williams, I.S., Buick, I.S., Cartwright, I., 1996. An extended episode of early Mesoproterozoic metamorphic fluid flow in the Reynolds Range, central Australia. *Journal of Metamorphic Geology* 14, 29–49.
- White, J.R., Chappell, B.W., 1977. Ultrametamorphism and granitoid genesis. *Tectonophysics* 43, 7–22.
- White, N.C., 2002. Introduction to the metallogeny and ore deposits of Asia: Mineral Potential of Asia: a forum on Asian metallogeny and ore deposits, exploration and development potential, regulatory and investment climate, and management practicalities. Metal Mining Agency of Japan, pp 5–6 with CD-ROM.
- Wu, Q.S., Xu, J.Z., Yang, Z., 1984. Sr isotopic characteristics of Gejiu Sn-bearing Granites and a study of ore search indicators. *Geochimica* 4, 293–302 (in Chinese with English abstract).
- Wu, F.Y., Jahn, B.M., Wilde, S.A., Lo, C.H., Yui, T.F., Lin, Q., Ge, W.C., Sun, D.Y., 2003. Highly fractionated I-type granites in NE China (I): Geochronology and petrogenesis. *Lithos* 66, 241–273.
- Wu, F.Y., Yang, Y.H., Xie, L.W., Yang, J.H., Xu, P., 2006. Hf isotopic compositions of the standard zircons and baddeleyites used in U-Pb geochronology. *Chemical Geology* 234 (1–2), 105–126.
- Xiao, C.H., Shen, Y.K., Wei, C.S., Su, X.K., Le, X.W., Zhang, L., 2018a. LA-ICP-MS Zircon U-Pb Dating, Hf Isotopic Composition and Ce⁴⁺/Ce³⁺ Characteristics of the Yanshanian Acid Magma in the Xidamingshan Cluster, Southeastern Margin of the Youjiang Fold Belt, Guangxi. *Geoscience* 32, 289–304 (in Chinese with English abstract).
- Xiao, C.H., Shen, Y.K., Liu, H., Wei, C.S., Le, X.W., Fu, B., 2018b. Oxygen isotopic compositions and geological significance of zircons from the Yanshanian felsic intrusions in the Xidamingshan cluster, southeastern margin of the Youjiang fold belt, South China: In-situ SHRIMP analysis, *Acta Petrol. Sin.* 34, 1441–1452 (in Chinese with English abstract).
- Xiao, C.H., Liu, H., Shen, Y.K., Wei, C.S., Le, X.W., Ou, D.G., Zhang, L., 2018c. Lead isotope geochemical characteristics of Xidamingshan ore concentration area on the southeastern margin of Youjiang fold belt, and their significance. *Miner. Deposits* 37 (5), 1037–1051 (in Chinese with English abstract).
- Xu, K.Q., Sun, N., Wang, D.Z., Ye, J., 1984. Geology of granites and their metallogenetic relations. Science Press, Beijing, 1–31 (in Chinese with English abstract).
- Yang, J.H., Peng, J.T., Hu, R.Z., Bi, X.W., Zhao, J.H., Fu, Y.Z., Shen, N.P., 2013. Garnet geochemistry of tungsten-mineralized Xihuashan granites in South China. *Lithos* 177, 79–90.
- Yang, F., Feng, Z.H., Kang, Z.Q., Xiao, R., 2011. Muscovite $^{40}\text{Ar}/^{39}\text{Ar}$ age of the Damingshan tungsten deposit in central Guangxi and its geological significance. *Geol. Bull. China* 30 (9), 1429–1433 (in Chinese with English abstract).

- Yang, F.Q., Lu, S.H., Li, H.L., Zhu, G.Q., Lu, X.L., Shi, W.M., 2017. On the spatial form of concealed rock mass in Xidamingshan area of Guangxi. Miner. Resour. Geol. 31, 1133–1140 (in Chinese with English abstract).
- Yu, Y., Ouyang, F., Jia, Y.Z., 2014. Geochemical characteristics of Zhaibao copper deposit in Jinxiu. Guangxi. Acta Geol. Sin. 88, 58–59.
- Yuan, H.L., Gao, S., Liu, X.M., Li, H.M., Günther, D., Wu, F.Y., 2004. Accurate U-Pb age and trace element determinations of zircon by laser ablation inductively coupled plasma-mass spectrometry Geostand. Geanal. Res. 28, 353–370.
- Yuan, K.Q., 1990. Prediction of concealed granite and deep prospecting. Science Press, Beijing (in Chinese with English abstract).
- Yuan, S.D., Peng, J.T., Hu, R.Z., Bi, X.W., Qi, L., Li, Z.L., Li, X.M., Shuang, Y., 2008a. Characteristics of rare-earth elements (REE), strontium and neodymium isotopes in hydrothermal fluorites from the Bailashui tin deposit in the Furong ore field, southern Hunan Province, China. Chin. J. Geochem. 27, 342–350.
- Yuan, S.D., Peng, J.T., Hu, R.Z., Li, H.M., Shen, N.P., Zhang, D.L., 2008b. A precise U-Pb age on cassiterite from the Xianghualing tin-polymetallic deposit (Hunan, South China). Miner. Deposits 43, 375–382.
- Yuan, S.D., Peng, J.T., Li, X.Q., Peng, Q.L., Fu, Y.Z., Shen, N.P., Zhang, D.L., 2008c. Carbon, oxygen and strontium isotope geochemistry of calcites from the Xianghualing tin-polymetallic deposit. Hunan province. Acta Geol. Sin. 82, 1522–1530 (in Chinese with English abstract).
- Yuan, S.D., Mao, J.W., Cook, N.J., Wang, X.D., Liu, X.F., Yuan, Y.B., 2015. A Late Cretaceous tin metallogenic event in Nanling W-Sn metallogenic province: constraints from U-Pb, Ar-Ar geochronology at the Jiepailing Sn-Be-F deposit, Hunan, China. Ore Geology Reviews 65, 283–293.
- Yuan, S.D., Peng, J.T., Hao, S., Li, H.M., Geng, J.Z., Zhang, D.L., 2011. In situ LA-MC-ICP-MS and ID-TIMS U-Pb geochronology of cassiterite in the giant Furong tin deposit, Hunan Province, South China: new constraints on the timing of tin-polymetallic mineralization. Ore Geol. Rev. 43, 235–242.
- Zhang, F.R., Shu, L.S., Wang, D.Z., Yu, J.H., Shen, W.Z., 2009. Discussion on the tectonic setting of Caledonian granitoids in the eastern segment of South China. Earth Sci. Front. 16, 248–260 (in Chinese with English abstract).
- Zhang, B.H., Ding, J., Ren, G.M., Zhang, L.K., Shi, H.Z., 2012. Geochronology and geochemical characteristic of the Lajunshan granites in Maguan County, Yunnan Province, and its geological implications. Acta Geol. Sin. 86, 587–601 (in Chinese with English abstract).
- Zhang, H.Q., Fu, W., Feng, Z.H., Long, M.Z., Li, B.Y., Li, W., Yue, X.J., Zheng, J.F., Li, S., Li, C., Wen, S.M., 2015. Discovery of strata-bound skarns and mineralization significance in Luowei mining area, Xidamingshan, Guangxi. J. Guilin Univ. Technology 35, 712–720 (in Chinese with English abstract).
- Zhao, Y.M., Li, D.X., 1987. Metasomatism in granite contact in Gejiu tin deposits, Yunnan Province. J. Chin. Acad. Geosci. 16, 237–252 (in Chinese with English abstract).
- Zhao, W.W., Zhou, M.F., Li, Y.H.M., Zhao, Z., Gao, J.F., 2017a. Genetic types, mineralization styles, and geodynamic settings of Mesozoic tungsten deposits in south China. J. Asian Earth Sci. 137, 109–140.
- Zhao, P.L., Yuan, S.D., Mao, J.W., Santosh, M., Zhang, D.L., 2017b. Zircon U-Pb and Hf-O isotopes trace the architecture of polymetallic deposits: A case study of the Jurassic ore-forming porphyries in the Qin-Hang metallogenic belt, China. Lithos 292–293, 132–145.
- Zhao, P.L., Yuan, S.D., Mao, J.W., Yuan, Y.B., Zhao, H.J., Zhang, D.L., Shuang, Y., 2018. Constraints on the timing and genetic link of the large-scale accumulation of proximal W-Sn-Mo-Bi and distal Pb-Zn-Ag mineralization of the world-class Dongpo orefield, Nanling Range, South China. Ore Geol. Rev. 95, 1140–1160.
- Zhong, L.F., Li, J., Peng, T.P., Xia, B., Liu, L.W., 2013a. Zircon U-Pb geochronology and Sr-Nd-Hf isotopic compositions of the Yuanzhuding granitoid porphyry within the Shihang Zone, South China: petrogenesis and implications for Cu-Mo mineralization. Lithos 177, 402–415.
- Zhong, L.F., Xia, B., Liu, L.W., Li, J., Lin, X.G., Xu, L.F., Lin, L.Z., 2013b. Metallogenic geochronology of Yuanzhuding Cu-Mo deposit in western Guangdong-eastern Guangxi metallogenic belt and its geological significance. Miner. Deposits 29, 395–404 (in Chinese with English abstract).
- Zhou, Y.J., Huang, H.S., 1997. Discussion on the (metal) mineralizing specialization of granite-about the relationships between granite and gold deposit. Gold Geol. 4, 15–21 (in Chinese with English abstract).
- Zhou, X.M., Li, W.X., 2000. Origin of Late Mesozoic igneous rocks in Southeastern China: implications for lithosphere subduction and underplating of mafic magmas. Tectonophysics 326, 269–287.
- Zhou, Y.Z., Zeng, C.Y., Li, H.Z., An, Y.F., Liang, J., Lv, W.C., Yang, Z.J., He, J.G., Shen, W.J., 2012. Geological evolution and ore-prospecting targets in southern segment of Qinzhou Bay-Hangzhou Bay juncture orogenic belt, southern China. Geological Bulletin of China 31, 486–491 (in Chinese with English abstract).
- Zhou, Y.Z., Zheng, Y., Zeng, C.Y., Liang, J., 2015. On the understanding of Qinzhou Bay-Hangzhou Bay metallogenic belt, South China. Earth Science Frontiers 22, 1–6 (in Chinese with English abstract).
- Zhu, G.F., 1989. The west Damingshan buried structures and intrusive, Guangxi province, and their relationship with mineral resources distribution. Geol. Prospecting 1, 15–17 (in Chinese with English abstract).
- Zhu, R.Z., Lai, S.C., Qin, J.F., Zhao, S.W., Santosh, M., 2018. Strongly peraluminous fractionated S-type granites in the Baoshan Block, SW China: Implications for two-stage melting of fertile continental materials following the closure of Bangong-Nujiang Tethys. Lithos 316–317, 178–198.